



OPEN ACCESS

Edited by:Alain Prochiantz,
Collège de France, France**Reviewed by:**Carlos Vicario,
Spanish National Research Council
(CSIC), Spain
Martine Cohen-Salmon,
INSERM U1050 Centre
Interdisciplinaire de Recherche en
Biologie, France***Correspondence:**Marysia Placzek
m.placzek@sheffield.ac.uk† These authors have contributed
equally to this work**‡ Present addresses:**Charlotte Muir,
School of Physiology, University of
Bristol, Bristol, United Kingdom
Marco Travaglio,
Medical Research Council (MRC)
Toxicology Unit, University of
Cambridge, Cambridge,
United Kingdom**Specialty section:**This article was submitted to
Neurodevelopment,
a section of the journal
Frontiers in Neuroscience**Received:** 10 December 2021**Accepted:** 27 January 2022**Published:** 07 April 2022**Citation:**Moore A, Chinnaiya K, Kim DW,
Brown S, Stewart I, Robins S,
Dowsett GKC, Muir C, Travaglio M,
Lewis JE, Ebling F, Blackshaw S,
Furley A and Placzek M (2022) Loss
of Function of the Neural Cell
Adhesion Molecule NrCAM Regulates
Differentiation, Proliferation
and Neurogenesis in Early Postnatal
Hypothalamic Tanycytes.
Front. Neurosci. 16:832961.
doi: 10.3389/fnins.2022.832961

Loss of Function of the Neural Cell Adhesion Molecule NrCAM Regulates Differentiation, Proliferation and Neurogenesis in Early Postnatal Hypothalamic Tanycytes

Alex Moore^{1,2,3†}, Kavitha Chinnaiya^{1,2,3†}, Dong Won Kim⁴, Sarah Brown^{1,2,3},
Iain Stewart^{1,2,3}, Sarah Robins^{1,2,3}, Georgina K. C. Dowsett^{5,6}, Charlotte Muir^{6†},
Marco Travaglio^{6†}, Jo E. Lewis^{5,6}, Fran Ebling⁶, Seth Blackshaw^{4,7,8,9,10}, Andrew Furley^{1,2,3}
and Marysia Placzek^{1,2,3*}¹ School of Biosciences, The University of Sheffield, Sheffield, United Kingdom, ² Bateson Centre, The University of Sheffield, Sheffield, United Kingdom, ³ Neuroscience Institute, The University of Sheffield, Sheffield, United Kingdom, ⁴ Solomon H. Snyder Department of Neuroscience, Johns Hopkins University School of Medicine, Baltimore, MD, United States, ⁵ Wellcome Trust-Medical Research Council Institute of Metabolic Science-Metabolic Research Laboratories, University of Cambridge, Cambridge, United Kingdom, ⁶ School of Life Sciences, University of Nottingham, Nottingham, United Kingdom, ⁷ Department of Ophthalmology, Johns Hopkins University School of Medicine, Baltimore, MD, United States, ⁸ Department of Neurology, Johns Hopkins University School of Medicine, Baltimore, MD, United States, ⁹ Institute for Cell Engineering, Johns Hopkins University School of Medicine, Baltimore, MD, United States, ¹⁰ Kavli Neuroscience Discovery Institute, Johns Hopkins University School of Medicine, Baltimore, MD, United States

Hypothalamic tanycytes are neural stem and progenitor cells, but little is known of how they are regulated. Here we provide evidence that the cell adhesion molecule, NrCAM, regulates tanycytes in the adult niche. NrCAM is strongly expressed in adult mouse tanycytes. Immunohistochemical and *in situ* hybridization analysis revealed that NrCAM loss of function leads to both a reduced number of tanycytes and reduced expression of tanycyte-specific cell markers, along with a small reduction in tyrosine hydroxylase-positive arcuate neurons. Similar analyses of NrCAM mutants at E16 identify few changes in gene expression or cell composition, indicating that NrCAM regulates tanycytes, rather than early embryonic hypothalamic development. Neurosphere and organotypic assays support the idea that NrCAM governs cellular homeostasis. Single-cell RNA sequencing (scRNA-Seq) shows that tanycyte-specific genes, including a number that are implicated in thyroid hormone metabolism, show reduced expression in the mutant mouse. However, the mild tanycyte depletion and loss of markers observed in NrCAM-deficient mice were associated with only a subtle metabolic phenotype.

Keywords: tanycyte, NrCAM, neural cell adhesion molecules, scRNA seq, radial glia, astrocytes, hypothalamus, neurogenesis

INTRODUCTION

The hypothalamus is the central regulator of organism-wide homeostasis and underpins numerous processes that support life, including feeding behavior, energy balance, sexual behavior and reproduction, aggression, and response to stress (Lechan and Toni, 2016). Situated around the third ventricle (3V) at the base of the forebrain, its neurons are found both within dense nuclei and more sparse areas that extend from the supraoptic region at the anterior border to the mammillary bodies at the posterior border. At the ventral surface of the mediobasal/tuberal hypothalamus, the median eminence (ME) and neurohypophysis/posterior pituitary bulge ventrally out of the hypothalamic pial surface, forming critical interfaces between the brain and the peripheral circulation.

Tanycytes—specialized Nestin-positive radial glial-like cells whose soma line the lateral and ventral walls of the 3V—are key to the ability of the ME to support the two-way flow of information from body-to-brain and brain-to-body (Prevot et al., 2018; Rodríguez et al., 2019). Four distinct tanycyte subsets are recognized (α 1-, α 2-, β 1- and β 2-tanycytes) (Rodríguez et al., 2019) that have been classified according to dorso-ventral (D-V) position, morphology, and marker expression—as well as through single-cell RNA sequencing (scRNA-Seq). Further, in rodents, different tanycyte subsets have been classified according to function. Distinct tanycyte subsets have been shown to regulate hormone levels, act as nutrient and hormone sensors, and regulate body content—all of which support acute physiological changes (Samms et al., 2015; Lazutkaite et al., 2017; Müller-Fielitz et al., 2017; Farkas et al., 2020; Yoo et al., 2020; Rohrbach et al., 2021).

In addition, studies in mice show that tanycytes may regulate long-term changes to hypothalamic neural circuitry through their ability to act as stem and progenitor cells (Lee et al., 2012, 2014; Robins et al., 2013; Yoo et al., 2021). Lineage-tracing and genetic ablation studies *in vivo*, and neurospherogenic studies *ex vivo*, support the idea that α 2-tanycytes are stem-like cells, and that other tanycyte subsets are progenitor-like cells (Robins et al., 2013; Yoo et al., 2021). While tanycytes can be experimentally forced into a neurogenic phase, the levels of tanycyte-derived neurogenesis are extremely low under baseline conditions in adult mouse, and the extent and physiological importance of tanycyte-derived neurogenesis in response to stimuli such as high-fat diet or psychological stress remains unclear (Yoo and Blackshaw, 2018). Further, as yet, little is known about the control of stem-like tanycytes. In other stem cell niches within the brain, cues provided by the local microenvironment ensure a fine balance that supports the sustained self-renewal of multipotent stem-like cells with the generation of progenitor cells and differentiated neurons (Silva-Vargas et al., 2013; Bjornsson et al., 2015). This balance allows continuous neurogenesis without depletion of the neural stem cell (NSC) pool and is tightly regulated. To date, it is unclear what factors support the maintenance of stem-like hypothalamic tanycyte cells.

Increasingly, studies have begun to focus on the role of cell adhesion molecules (CAMs) in regulating NSCs within their niche (Hynes, 2002; Marthiens et al., 2010; Hu et al., 2017; Morante-Redolat and Porlan, 2019). CAMs from the cadherin,

integrin, selectin, and immunoglobulin families are expressed within neurogenic regions of the adult brain (Chen et al., 2013), and members of the immunoglobulin superfamily of CAMs (Ig-SF CAMs) have been shown to play roles in the regulation of neural progenitors (Gennarini et al., 2017). However, while CAMs can regulate acute physiological functions in tanycytes (Messina and Giacobini, 2013; Parkash et al., 2015), no study has yet asked whether CAMs regulate the stem/progenitor-like behavior of tanycytes.

The L1-like family of CAMs are a prominent subgroup of Ig-SF CAMs that play a wide range of roles in neuronal differentiation (Maness and Schachner, 2007). In addition, LICAMs, including the family member NrCAM (NgCAM-related cell adhesion molecule/neuronal cell adhesion molecule), modulate neural cell proliferation. In mouse, loss of NrCAM leads to a reduction in cerebellar lobe size, while L1/NrCAM double mutants show major reductions in cerebellar size (Sakurai et al., 2001; Heyden et al., 2008; Zonta et al., 2011). A role for NrCAM in controlling cell proliferation is further implied from its involvement in tumorigenesis, where it has been linked to increased proliferation and motility in melanoma and colorectal cancers (Conacci-Sorrell et al., 2002, 2005; Chan et al., 2011).

Previous studies have suggested expression of NrCAM in the ventricular zone (VZ) of both the developing (Edwards et al., 1990; Lustig et al., 2001; Noctor et al., 2001; Tamamaki et al., 2001; Sild and Ruthazer, 2011) and the adult mouse hypothalamus (Lein et al., 2007), although no detailed analysis has been described. Furthermore, both studies of NrCAM-null mice and genomic association studies have linked NrCAM with impaired sociability, addiction and autism, conditions associated with hypothalamic dysfunction (Ishiguro et al., 2006, 2014, 2019; Sakurai et al., 2006; Moy et al., 2009; Sakurai, 2012). As yet, though, no study has systematically analyzed the expression or potential function of NrCAM in the hypothalamus.

Here we describe the cellular expression pattern of NrCAM in the hypothalamus of 8–10 week adult mice. NrCAM is detected in all four tanycyte subsets and in hypothalamic astrocytes. In hypothalamic neurospheres, NrCAM is coexpressed with hypothalamic stem/progenitor-like regional markers, indicating that it marks tanycyte stem/progenitor cells. Loss of NrCAM (NrCAM KO) leads to a small but significant loss of tanycytes and reduction in expression of tanycyte markers, a thinning of the VZ, and a modest but statistically significant reduction in tyrosine hydroxylase (TH)-positive neurons in the postnatal period. Further, *ex vivo* assays show that tanycytes derived from NrCAM KO mice show decreased proliferation and generate smaller numbers of GFAP-positive astrocytes and TH-positive neurons. ScRNA-Seq of hypothalamic tissue from wild-type and NrCAM KO littermates confirms that NrCAM is highly expressed in tanycytes and astrocytes. In the tanycyte-cell fraction of NrCAM KO mice, tanycyte-specific genes, including a number that are implicated in thyroid hormone metabolism, show reduced expression, while astrocyte-specific genes show increased expression. In contrast, expression of astrocyte-specific markers are reduced in mutant astrocytes. We also detect altered expression of some GABAergic markers and *Trh* in hypothalamic neurons. NrCAM KO mice showed a small but significant reduction in body weight compared to wild-type littermates,

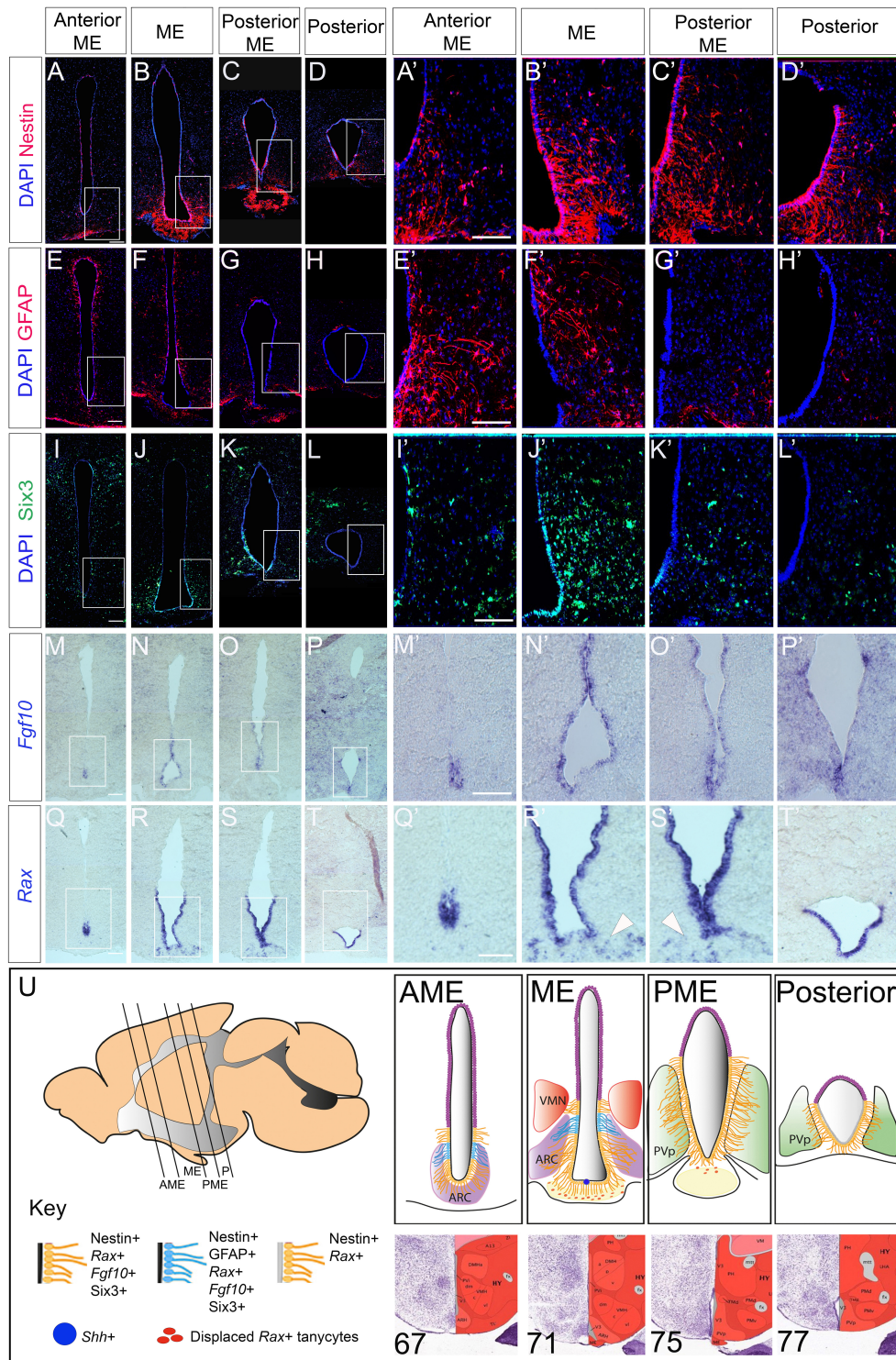


FIGURE 1 | Stem and progenitor marker distribution in the adult hypothalamus. **(A–L)** Representative examples from consecutive coronal sections, from anterior to posterior, at the level of the AME, ME, PME and posterior tanyocyte-rich hypothalamus; serial adjacent sections analyzed for expression of Nestin, GFAP and Six3. Boxed regions in panels **(A–D, E–H, I–L)** shown at high power in panels **(A'–D', E'–H', I'–L')** ($n = 5$ mice; images from a single mouse). **(M–T)** Representative examples from consecutive coronal sections across the AME, ME, PME and posterior tanyocyte-rich hypothalamus; serial adjacent sections analyzed for expression of *Fgf10* and *Rax*. Boxed regions in panels **(M–P, Q–T)** shown at high power in panels **(M'–P', Q'–T')**. Arrowheads in panels **(R', S')** point to *Rax*-expressing displaced tanyocytes ($n = 3$ mice; images from a single mouse). **(U)** Schematics showing tanyocyte heterogeneity along the A-P axis.

(Continued)

FIGURE 1 | approximate section planes and positions of tanycytes in AME, ME, PME and posterior regions. Coronal schematics show extent of tanycytes of different character along the A-P axis. See key for details. Positions of the AME, ME, PME and posterior were judged relative to sections in the ABRA, based on morphology and position of key nuclei: specific numbered sections from the ABRA are shown below each schematic. Scale bar: 100 μ m. ARC, arcuate nucleus; AME, anterior to median eminence; ME, median eminence, PME, posterior median eminence; P, posterior tanycyte-rich hypothalamus; PVP, periventricular nucleus, posterior part; VMN, ventromedial nucleus.

which was associated with reduced food intake, but not with altered locomotor activity or energy expenditure. In summary, NrCAM is a novel surface marker of hypothalamic tanycytes and may regulate cellular homeostasis in and around the 3V. However, the mild tanycyte depletion and loss of markers observed in NrCAM KO mice were associated with only a subtle metabolic phenotype.

RESULTS

Stem and Progenitor Cell Marker Distribution in the Adult Hypothalamus

We systematically analyzed Nestin-positive tanycyte distribution over a 1,000 μ m length in and around the ME, corresponding approximately to Bregma position -0.9 to -2.2 in the intact skull. From anterior to posterior, tanycytes are first detected around the ventral-most VZ, anterior to the morphologically-distinct ME [a region we term the anterior ME (AME), corresponding to sections 67–68 in the Allen Brain Reference Atlas (ABRA)] (**Figures 1A,A',U**). Over the length of the ME (corresponding to sections 69–73 in the ABRA) they increase in density and extend further dorsally (**Figures 1B,B',U**). Tanycytes continue to line the 3V in the posterior ME (PME) (sections 74–75 in the ABRA) and a more posterior region adjacent to the periventricular nucleus (posterior part) (sections 76, 77 in the ABRA) (**Figures 1C,D,C',D',U**). At all positions, Nestin is detected strongly in $\beta 1/2$ tanycytes, and more weakly in dorsal $\alpha 1/2$ tanycytes. Direct comparison of Nestin and GFAP, the latter a marker of $\alpha 2$ -tanycytes, confirms that GFAP-positive $\alpha 2$ -tanycytes – previously implicated as stem-like cells – lie dorsal to β tanycytes and shows that GFAP-positive tanycytes are largely detected in the AME and ME (**Figures 1E–H'**).

We next asked how the gene expression profile of tanycytes compares to that of other known hypothalamic stem/progenitor markers. Direct comparison of Nestin and *Six3* shows that in the VZ, *Six3* is largely confined to ME regions with little/no expression detected in AME or posterior regions (**Figures 1I–L'**). *Fgf10*—implicated in the control of tanycyte proliferation (Robins et al., 2013)—is expressed in the VZ in the AME, ME and PME, but is barely detected in the posterior hypothalamus (**Figures 1M–P'**). By contrast, *Rax*—a transcription factor necessary for tanycyte differentiation (Miranda-Angulo et al., 2014; Salvatierra et al., 2014)—is expressed throughout tanycyte-rich regions in the AME, ME, PME and posterior hypothalamus (**Figures 1Q–T'**). In addition, *Rax* is detected in ME cells beneath the VZ—previously described as displaced tanycytes (Miranda-Angulo et al., 2014) (**Figures 1R',S'** arrowheads). In the embryo, *Six3*, *Rax* and *Fgf10* all modulate the activity of the signaling ligand *Shh* to direct differentiation of anterior tuberal progenitor

cells (Kano et al., 2019; Farkas et al., 2020; Placzek et al., 2020). This, and the overlap of *Six3/Rax/Fgf10* in the adult, prompted us to examine expression of *Shh* in the adult hypothalamus. *Shh* was detected, but confined to a tiny subset of cells, occupying the midline in the ME/PME (**Supplementary Figure 1**). Together these analyses show a previously undescribed profile of tanycyte distribution along the A-P axis (schematized in **Figure 1U**).

NrCAM Is Expressed on Tanycytes

We next examined the profile of NrCAM. Double-labeling of consecutive sections with Nestin and NrCAM reveals that NrCAM is expressed in tanycytes throughout the AME, ME, PME and posterior hypothalamus (**Figures 2A–D**). At all positions, NrCAM is detected strongly on tanycyte cell bodies and more weakly on tanycyte processes (**Figures 2A–H'**), which appear fasciculated (**Figure 2I**). While there is some variation in expression levels of Nestin and NrCAM in different tanycyte subsets (e.g., **Figure 2E**), quantitative analyses of high power views suggest similar numbers of Nestin-positive and NrCAM-positive tanycytes (**Figures 2J–K**).

The particularly strong expression of NrCAM on $\alpha 2$ tanycyte cell bodies (**Figures 2B,C**) prompted us to explore whether NrCAM marks these cells as they undergo self-renewal. To do so we took advantage of previous work, which had shown that stem-like $\alpha 2$ tanycytes can be cultured as neurospheres, up to and beyond the seventh passage (Robins et al., 2013). Using this assay, we analyzed 7th passage neurospheres, cultured under non-differentiated conditions (**Figure 2L**). Neurospheres expressed NrCAM, which was detected on every cell (**Figure 2M**), as were the neural stem-like markers *Slc1a3* and *Sox2* (**Figures 2N,O**). At the same time, neurospheres expressed the hypothalamic stem/progenitor-like regional markers, *Six3/Six3* and *Nkx2-1/Nkx2-1* but did not express *Pax6* or *Nkx6-1*—markers of non-hypothalamic progenitor subtypes (**Figures 2P–R** and **Supplementary Figure 2**). Expression of *Six3* was specific to hypothalamic-derived neurospheres and was not detected on neurospheres obtained from the subventricular zone (SVZ) of the lateral ventricle or spinal cord ependymal cells (**Supplementary Figure 2**). Under differentiation conditions, NrCAM became restricted to central-most portions of neurospheres (**Figure 2S**). Together this suggests that NrCAM marks tanycyte stem/progenitor cells.

Loss of NrCAM Depletes Hypothalamic Tanycytes Postnatally

To determine if loss of NrCAM leads to a reduction in tanycyte number *in vivo*, we compared tanycyte process distribution and tanycyte progenitor marker expression in week 8–10 NrCAM KO mice—in which NrCAM protein cannot be detected (**Supplementary Figures 3A,B**; Sakurai et al., 2001)—and

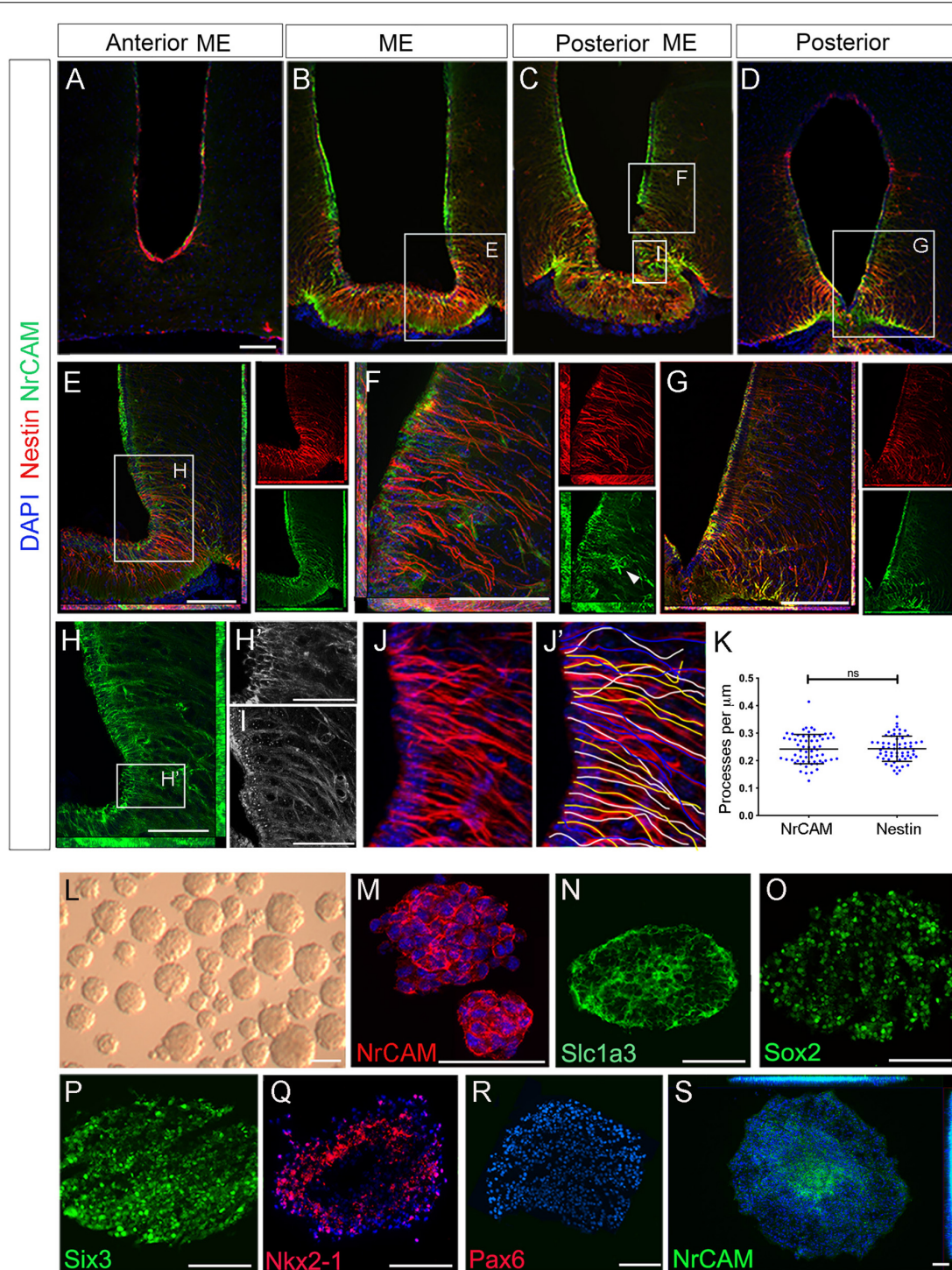


FIGURE 2 | NrCAM is expressed on self-renewing hypothalamic tancytes. (A–D) Consecutive coronal sections at the level of the AME, ME, PME and posterior tancyte-rich hypothalamus, from a single mouse, double-labeled to detect expression of Nestin and NrCAM. (E–G) High power views of boxed regions in panels (B–D) shown as double or single channel views. Arrowhead in panel (F) (single channel green) points to an NrCAM-positive astrocyte. (H) High power view of boxed region in panel (E). Single channel view shows NrCAM labeling. Panel (H') shows high power view of boxed region in panel (H) showing high expression of NrCAM on tancyte cell bodies. (I) High power view of boxed region in panel (C) shows NrCAM labeling appears fasciculated on tancytes. (J–K) Quantification of Nestin and NrCAM-positive process density. Sections through the hypothalamus were imaged at 40x (J) and individual tancytes traced (J'). Quantitative analysis (K) shows no significant difference across the entire hypothalamus ($p < 0.0001$; unpaired t -test) ($n = 3$ mice). (L–S) 7th passage neurospheres derived from VZ around 3V, analyzed in brightfield (L) or after immunohistochemical analyses (M–S) after culture under non-differentiation (M–R) or differentiation (S) conditions ($n = 15-20$ neurospheres/condition). Scale bars: (A–H) 100 μm ; (H', I) 45 μm ; (M–S) 50 μm .

wild-type littermates. Analysis of Nestin expression across the hypothalamus shows that fewer processes are seen in the AME, ME, PME, and P regions in NrCAM KO animals in comparison to WT animals (Figures 3A,B). Quantification of process density (analysis restricted to regions harboring β 1- and α 2-tanycytes) showed a statistically significant decrease in process density across the whole hypothalamus (Figure 3K); consistently, each subregion showed an \sim 20% decrease in the number of Nestin-positive processes (Figure 3L). Analysis of GnRH, which decorates tanycyte processes, likewise points to a decrease in density of tanycyte processes (Supplementary Figures 3C,D). Analysis of the α 2-tanycyte region, at the level of the ME (boxed region in Figures 3A,B) showed that the reduction in Nestin is accompanied by a significant thinning of the VZ (Figures 3A',B',M) and a marked reduction in GFAP-positive process density (Figures 3A',B',N). Analysis of Six3 expression confirms the thinner VZ (Figures 3C-D',O). At the same time, *Rax* and *Fgf10* are expressed more weakly in NrCAM KO mice, and *Rax* shows a modest reduction in the length of its expression domain in the ME, compared to wild-type littermates (Figures 3E-H',P-S), while *Shh*-expressing cells are barely discernible (Supplementary Figures 3E',F',H,H'). This suggests that loss of NrCAM leads to a reduction in the generation and/or maintenance of tanycytes. Changes are not limited to ventricular cells, and we also note a significant reduction in the number of displaced *Rax*-positive tanycytes cells in the ME parenchyma (Figures 3E',F' arrowheads; Figure 3T) (Miranda-Angulo et al., 2014).

Previous studies have suggested that tanycytes can give rise to NPY-expressing neurons in the arcuate nucleus (Arc) (Haan et al., 2013; Yoo et al., 2021) and we therefore asked if the reduction in tanycytes in NrCAM KO mice is accompanied by a reduction in NPY neurons. Immunohistochemical analysis shows no change in area or intensity of NPY neurons in NrCAM KO vs. wild-type littermates (Supplementary Figures 3E,E',G,G'). However, we detect a small but significant decrease in TH-positive A12 Arc neurons in NrCAM KO vs. wild-type littermates (Figures 3I-J',U,V). The decrease in TH-positive neurons appears to be specific to the A12 population in the Arc region of the hypothalamus, as no significant difference was observed in the number of A13 TH-positive neurons of the zona incerta (Romanov et al., 2017; Supplementary Figure 3I,J).

Although these changes are consistent with the idea that NrCAM might play a role in cellular homeostasis within the hypothalamus, they could reflect a developmental phenotype: previous studies have shown that NrCAM is expressed in the hypothalamus in the E14 embryonic mouse (Lustig et al., 2001; Kim et al., 2020). Analysis of E16 mice, however, showed only a small decrease in density of radial glial processes, around the level of the emerging ME (Figures 4A,B,K and Supplementary Figure 4) and no difference in expression of *Rax*, *Six3* (Figures 4C-F,L,M,P), *Fgf10*, or *Shh* (Figures 4N,O and Supplementary Figure 4). *Lhx2*, which is expressed at high levels in radial glial cells in positions analogous to α -tanycytes of adult mice shows a small decrease at levels just posterior to the ME, but in other regions, is expressed similarly in the two genotypes (Figures 4G,H,Q), while TH-positive neurons in the region of the developing Arc were increased in NrCAM KO mice, relative

to wild-type littermates (Figures 4I,J,R analyzed at E18). The changes detected in 8–10 week mice therefore likely reflect an effect of NrCAM in the postnatal period.

Decreased Proliferation/Differentiation of NrCAM-Derived VZ/SVZ Tissues

To directly assay the function of tanycytes in NrCAM KO mice, we analyzed neurospherogenic potential of VZ cells harboring β 1/ β 2 and α 2 tanycytes. NrCAM KO hypothalamic tissue generated primary neurospheres that could be passaged. The number of secondary neurospheres formed from NrCAM KO was initially significantly higher than wild-type but later declined: by passage 7, the number of NrCAM KO neurospheres was significantly lower than wild-type neurospheres (Figure 5A). Neurospheres from NrCAM KO mice appeared smaller than wild-type neurospheres, and indeed, cell concentration was significantly reduced in NrCAM KO neurospheres compared to wild-type (Figure 5B). These observations support the hypothesis that there are fewer stem/progenitor cells in NrCAM KO mice.

To determine if neurospheres from NrCAM KO mice showed limited differentiation capacity, we subjected passage 6 neurospheres derived from NrCAM KO and wild-type littermates to differentiation conditions. As previously demonstrated (Robins et al., 2013), wild-type hypothalamic neurospheres can give rise to both glial-like cells (GFAP-positive, RIP-positive, and Nestin-positive cells) (Figures 5C,D,G) and hypothalamic neurons (MAP2, GHRH, NPY, TH) (Figures 5E,F,H). Similar cells were detected in neurospheres derived from NrCAM KO mice (Figures 5I-N), and, as in wild-type tissue, the neurospheres retained some progenitor-like hypothalamic markers (*Six3*). Generally, similar numbers of cells were detected in the two genotypes; however, fewer GFAP-positive astrocytes and fewer TH-positive neurons were detected in NrCAM KO neurospheres compared to wild-type (Figures 5C,H,I,N,O). These analyses show that astrocytes and TH neurons can be generated from postnatal tanycytes as previously reported (Robins et al., 2013; Yoo et al., 2021), and suggest that loss of NrCAM reduces generation of tanycyte-derived TH neurons.

Neurospheres, however, are cultured over a lengthy period, and so may be subject to culture artifacts. We therefore established an acute assay, to ask if we could see evidence for the *de novo* generation of TH-positive Arc neurons. VZ/SVZ tissue from the region of the ME was micro-dissected (Figures 5P,Q). We aimed to dissect tissue containing α 2 and β -tanycytes, and avoid more dorsal regions that would likely be contaminated with TH-positive neurons (Figures 5R,S). Accuracy of dissection/avoidance of TH-positive neurons was confirmed through immediate analysis of a subset of explants (Figure 5T). In parallel, a subset of explants was cultured. In cultured explants from both wild-type and NrCAM KO mice, we detected phosphoH3-positive proliferating cells and TH-positive neurons (Figure 5U). However, we detected significantly fewer TH-positive neurons in NrCAM KO tissue, compared to wild-type (Figure 5V). Together, the neurosphere and organotypic assays indicate that tanycytes from NrCAM KO mice have reduced ability to proliferate and differentiate.

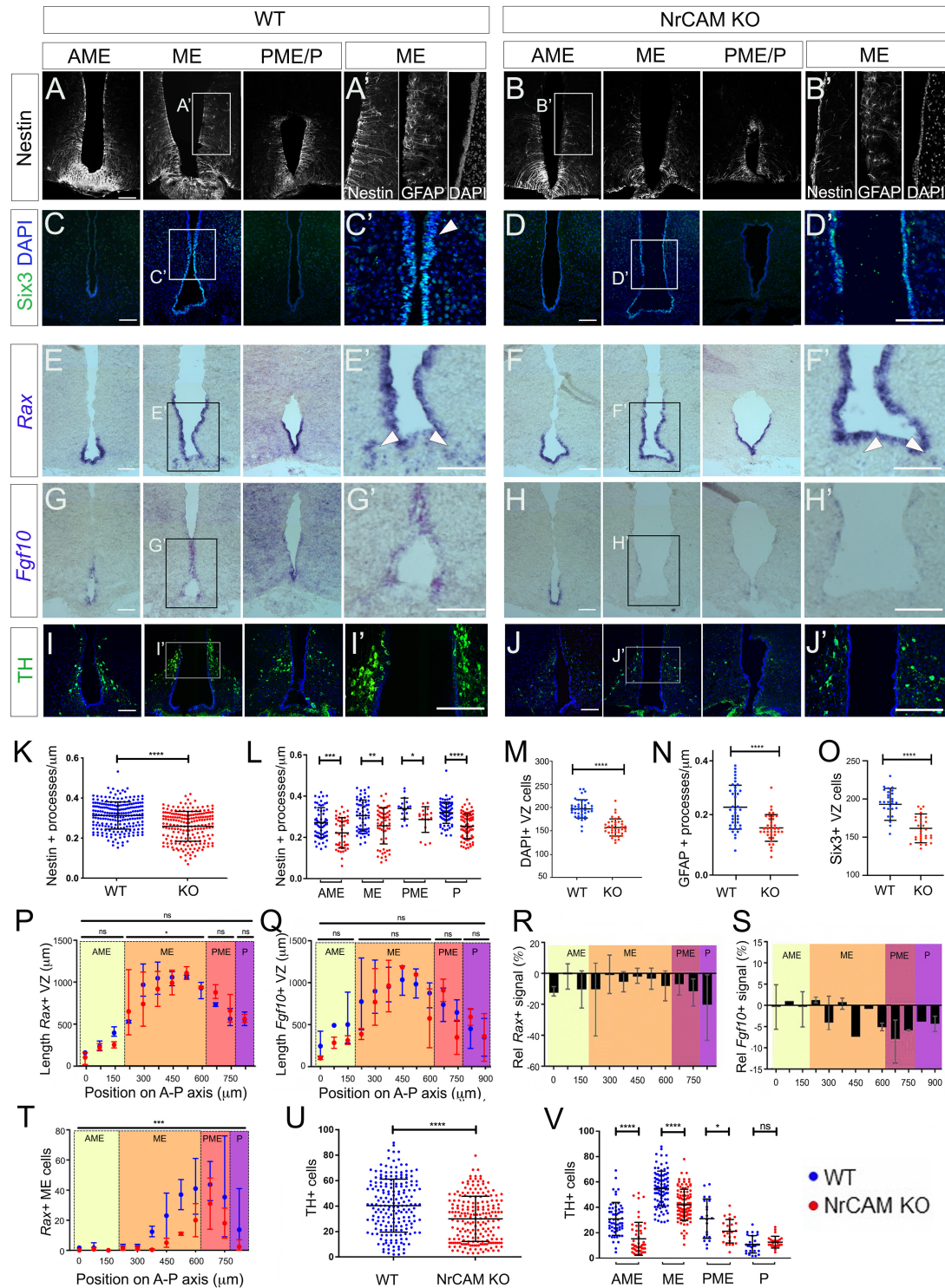


FIGURE 3 | Reduced tanyocytes and tyrosine hydroxylase (TH) neurons in the NrCAM KO adult. **(A–J)** Representative coronal sections through AME, ME and PME/P regions of the hypothalamus of wild-type **(A,C,E,G,I)** or NrCAM KO mice **(B,D,F,H,J)**. Panels **(A'–J')** show high power views of boxed regions in panels **(A–J)**. Sections were immunolabeled to detect Nestin **(A,B)**, Six3 **(C,D)**, TH **(I,J)**, or GFAP **(A',B')**: consecutive section to that analyzed for Nestin], or were analyzed by *in situ* hybridization to detect *Rax* **(E,F)** or *Fgf10* **(G,H)**. Arrowheads in panels **(C',D')** point to Six3-positive VZ cells and in panels **(E',F')** point to *Rax*-positive displaced tanyocyte cells [total of $n = 11$ mice/genotype analyzed for Nestin and GFAP ($n = 3$), TH ($n = 3$); *Rax* and *Fgf10* ($n = 3$); Six3 ($n = 2$)]; images in panels **(E,G)** show serial adjacent sections through a single mouse. Scale bars: 100 μm . **(K–L)** There is a significant *(Continued)*

FIGURE 3 | reduction in Nestin-positive $\beta 1$ - and $\alpha 2$ -tancyte density in NrCAM KO mice across the entire hypothalamus (**K**) ($p < 0.0001$; unpaired t -test) and across each subregion (**L**) (AME $p = 0.0007$; ME $p = 0.0013$; PME $p = 0.0105$; $p < 0.0001$; unpaired t -test) ($n = 3$ mice/genotype). (**M–O**) There is a significant reduction in the number of cells lining the VZ (**M**) ($p < 0.0001$; unpaired t -test; $n = 3$ mice/genotype), in GFAP-positive tancyte density (**N**) ($p < 0.0001$; unpaired t -test; $n = 3$ mice/genotype), and in Six3-positive nuclei in NrCAM KO mice (**O**) ($p < 0.0001$; unpaired t -test; $n = 2$ mice/genotype). (**P–T**) Quantitative analyses of *Rax* and *Fgf10*. Analysis was performed at 75 μm intervals across AME, ME, PME and P subregions in 3 mice/genotype. Each plotted value is the mean of the three biological replicates; bars show range. (**P,Q**) Lengths of *Rax*- and *Fgf10*-expressing domains in wild-type (blue) and NrCAM KO (red) mice and (**R,S**) percentage change in *Rax* and *Fgf10* signal strength in NrCAM KO relative to wild-type. *Rax*-expressing VZ was significantly longer in the ME subregion of wild-type mice (**P**) (Wilcoxon signed rank test; $p = 0.0273$). Relative intensity of *Rax* and *Fgf10* was reduced in NrCAM KO compared to wild-type mice at most levels (**R,S**). (**T**) Significantly fewer *Rax*-positive displaced tancytes were observed in the NrCAM KO compared to wild-type mice (Wilcoxon signed rank test; $p = 0.0010$). (**U,V**) There is a significant reduction in TH-positive cells in NrCAM KO mice across the entire hypothalamus (**U**) ($p < 0.0001$; unpaired t -test with Welch's correction) and across subregions (**V**) (AME $p < 0.0001$; ME $p < 0.0001$; PME $p = 0.0158$; unpaired t -test with Welch's correction). No significant difference was seen in the P subregion where ARC TH-positive cells are least populous ($p = 0.2865$). Each icon in each plot represents a single measurement (30 sections analyzed/mouse/genotype for Nestin and TH; 6–7 sections analyzed/mouse for Six3, GFAP, *Rax* and *Fgf10*). Bars in each plot show SD. Statistical significance denoted in charts by asterisks: * $p < 0.05$, ** $p < 0.01$, *** $p < 0.001$, **** $p < 0.0001$.

scRNA Comparison of NrCAM KO and Wild-Type Hypothalamic Tissue

To further identify molecular changes between wild-type and NrCAM KO, we performed scRNA-Seq on adult hypothalamus on both genotypes. This approach confirmed that *NrCAM* expression is detected in tancytes and astrocytes, but also detected expression in neurons and oligodendrocyte-precursor cells (OPC) (**Supplementary Figure 5**). We then sub-setted tancytes for further analysis, clustering these into $\alpha 1$ -, $\alpha 2$ -, $\beta 1$ - and $\beta 2$ subsets based on previously known molecular markers (**Figures 6A,B**; Yoo et al., 2021).

Similar to the immunohistochemical and *in situ* analyses, we detected subtle changes in gene expression. As expected, we observed a decrease in *Nrcam* expression in KO compared to wild-type control mice in each tancyte subset (**Figure 6C**) and a decrease in *Nestin* and *Rax* (**Figure 6C**), adding weight to the idea that tancytes are reduced in the NrCAM KO mouse. We also observed reduced levels of *Hes1* and *Prdx6*—both previously implicated in regulating the balance of radial glial-like neural stem cells and neurons elsewhere in the CNS (Bai et al., 2007; Park et al., 2016; Bosze et al., 2020) and reduced levels of *Metr*, a gene implicated in astrocyte differentiation (Nishino et al., 2004; **Supplementary Table 1**). Additionally, we observed lower levels of the tancyte-enriched genes, *Ndn*, *Crym* and *Gpr50*, previously shown to regulate thyroid hormone signaling (**Figure 6C** and **Supplementary Table 1**; Bechtold et al., 2012; Hasegawa et al., 2012; Kinney and Bloch, 2021). Finally, we detected a small increase in *Slc1a4*, *Slc1a2* (solute carrier family 1 member), *Ntsr2* (neurotensin receptor 2) and *Mal* (**Figure 6C** and **Supplementary Table 1**). These genes are not typically expressed, or expressed only at low levels, in tancytes, but are typically enriched in astrocytes (*Slc1a4*, *Slc1a2*, and *Ntsr2*) and oligodendrocytes (*Mal*). The loss of NrCAM therefore appears to lead to a modest upregulation of tancyte expression of genes specific to other glial cell types.

Previous lineage-tracing studies, showing that tancytes can give rise to astrocytes (Lee et al., 2012; Haan et al., 2013; Robins et al., 2013; Yoo et al., 2021), and the reduced numbers of GFAP-expressing astrocyte cells in differentiated neurospheres obtained from NrCAM KO compared to wild-type mice (**Figures 5C,I**) prompted us to perform further analyses of astrocytes from wild-type and NrCAM KO littermates. We observed marked molecular changes in astrocytes between wild-type and NrCAM

KO mice (**Supplementary Figure 6**). No NrCAM expression was detected and the classic astrocyte-enriched markers, *Ntsr2*, *Agt* (angiotensinogen), *Mt2* (metallothionein2), *Slc1a3* (solute carrier family 1 member 3), and *Gjal* (gap junction protein Connexin 43) were all expressed at lower levels in NrCAM KO compared to wild-type mice (**Supplementary Figure 6** and **Supplementary Table 2**). *Htra1*—which encodes a serine protease that regulates TGFbeta and the availability of insulin-like growth factors—and has been not previously identified as an astrocyte-enriched marker—was also reduced. At the same time, other genes were upregulated, including *Vimentin* (*Vim*—a tancyte-enriched intermediate filament-encoding gene), *Secretogranin* (*Scg2* involved in the packaging or sorting of peptide hormones and neuropeptides into secretory vesicles) and *Pfdn2* (**Supplementary Figure 6** and **Supplementary Table 2**). In summary, scRNA seq analysis shows that astrocytic markers are reduced in the NrCAM KO mouse.

Finally, we interrogated hypothalamic neurons. Distinct subclasses could be identified, based on known molecular markers (**Figure 7A**). Comparative analyses revealed a subtle decrease in expression levels of GABAergic neuron-associated genes (*Penk*, *Gabra1*, *Gria2*), the GABAergic marker (*Slc32a1*) as well as the glutamatergic marker (*Slc17a6*) in NrCAM KO mice, relative to wild-type littermates (**Figure 7B** and **Supplementary Table 3**). Additionally, we detected a small reduction in thyrotropin releasing hormone (*Trh*) (**Figure 7B** and **Supplementary Table 3**). However, the overall profile of neurons/neuronally-expressed genes was similar in mutant and wild-type mice. The decrease in tancytes and astrocytes in NrCAM KO mice, therefore, does not lead to easily-detectable changes in hypothalamic neuronal profiles.

Behavioral Assays

The scRNA seq experiments suggest, nonetheless, that genes that govern thyroid hormone activity (*Trh*, *Ndn*, *Crym*, *Gpr50*) are subtly reduced in the NrCAM KO mice. Given the central role of thyroid hormone in metabolism, we therefore investigated whole body physiology in NrCAM KO mice vs. wild-type (littermate) control animals. Weight at birth was similar in NrCAM KO and wild-type mice, and in post-weaned juvenile mice (weeks 5 and 6) fed standard chow, food intake was similar (**Supplementary Figure 7**). However, thereafter, in mice fed standard chow, bodyweight in NrCAM KO was significantly reduced, as was

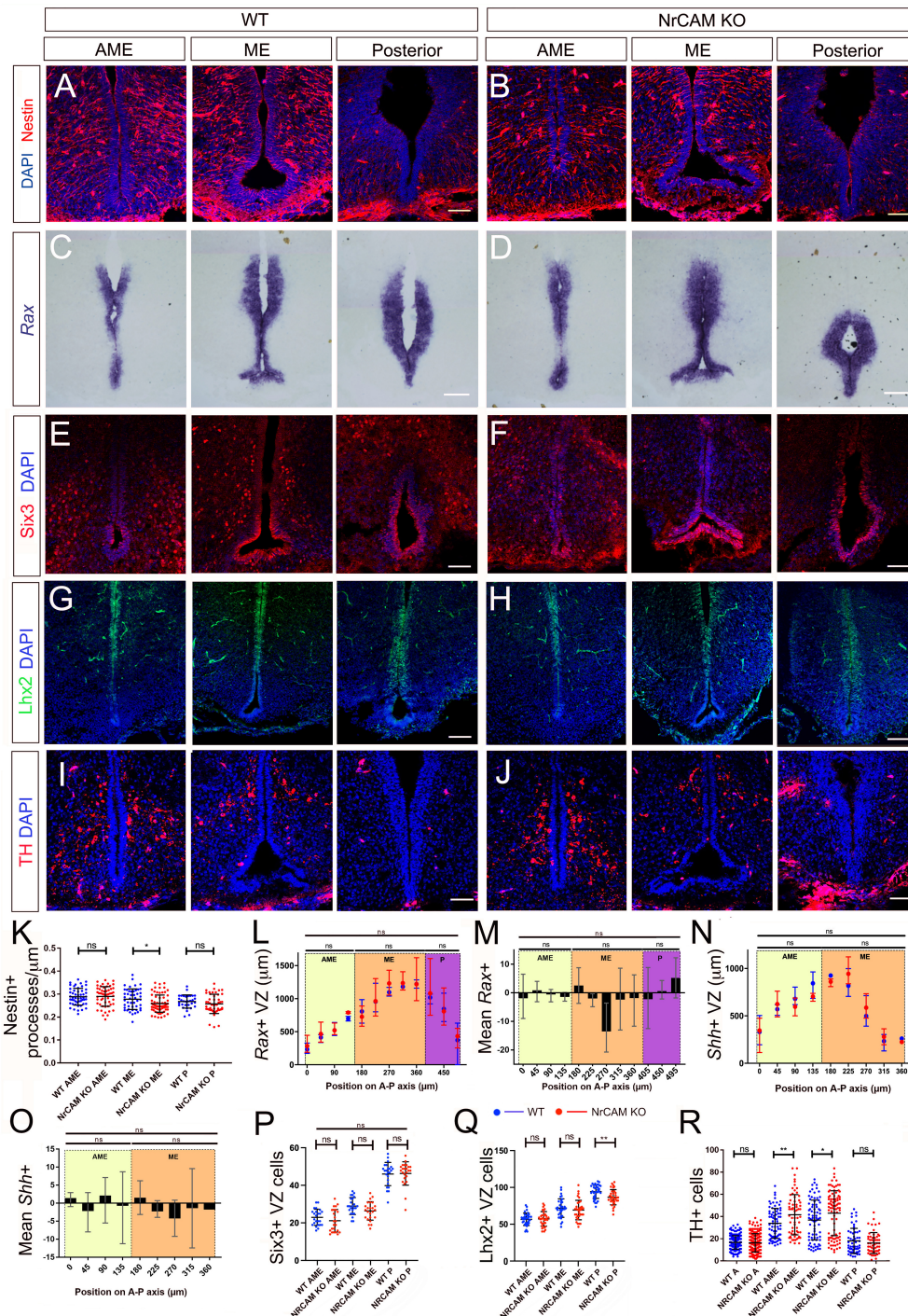


FIGURE 4 | Comparison of tanycytes and TH neurons in the embryo. **(A–H)** Representative serial coronal sections through AME, ME and posterior regions of the hypothalamus of E16 wild-type **(A,C,E,G)** or NrCAM KO mice **(B,D,F,H)** analyzed by immunohistochemistry to detect Nestin **(A,B)**, Six3 **(E,F)**, Lhx2 **(G,H)**, or by chromogenic *in situ* hybridization to detect *Rax* **(C,D)** ($n = 8$ mice/genotype, analyzed for Nestin ($n = 3$), Six3 ($n = 2$), Lhx2 ($n = 3$) or *Rax* ($n = 3$)). **(I,J)** Representative serial coronal sections through AME, ME and posterior regions of the hypothalamus of E18 wild-type **(I)** or NrCAM KO mice **(J)** analyzed by immunohistochemistry to detect TH ($n = 3$ mice/genotype). Scale bars: 100 μm . **(K–R)** Quantitative analyses in wild-type and NrCAM KO mice. **(K)** There is only a small reduction in Nestin-positive $\beta 1$ - and $\alpha 2$ -tanycyte density in NrCAM KO mice across the ME region ($p < 0.0200$; unpaired *t*-test). Each icon represents a single measurement ($n = 3$ mice/genotype). Bars show SD. **(L–P)** There is no significant reduction in the lengths or relative intensities of *Rax*- and *Shh*-expressing domain ($n = 3$ mice/genotype), nor in the number of Six3 + VZ cells in wild-type (blue) and NrCAM KO (red) mice ($n = 2$ mice/genotype). Bars in panels **(L,N)** show mean and range; in panels **(P–R)** each icon represents a single measurement; bars show SD. **(Q)** There is only a small reduction in the number of Lhx2 + VZ cells in NrCAM KO mice across the posterior region ($p = 0.002$; unpaired *t*-test) ($n = 3$ mice/genotype). **(R)** There is a small increase in TH-positive cells in NrCAM KO mice in the ME/AME (AME $p = 0.0044$; ME $p = 0.0390$) ($n = 3$ mice/genotype). Statistical significance denoted in charts by asterisks: * $p < 0.05$, ** $p < 0.01$.

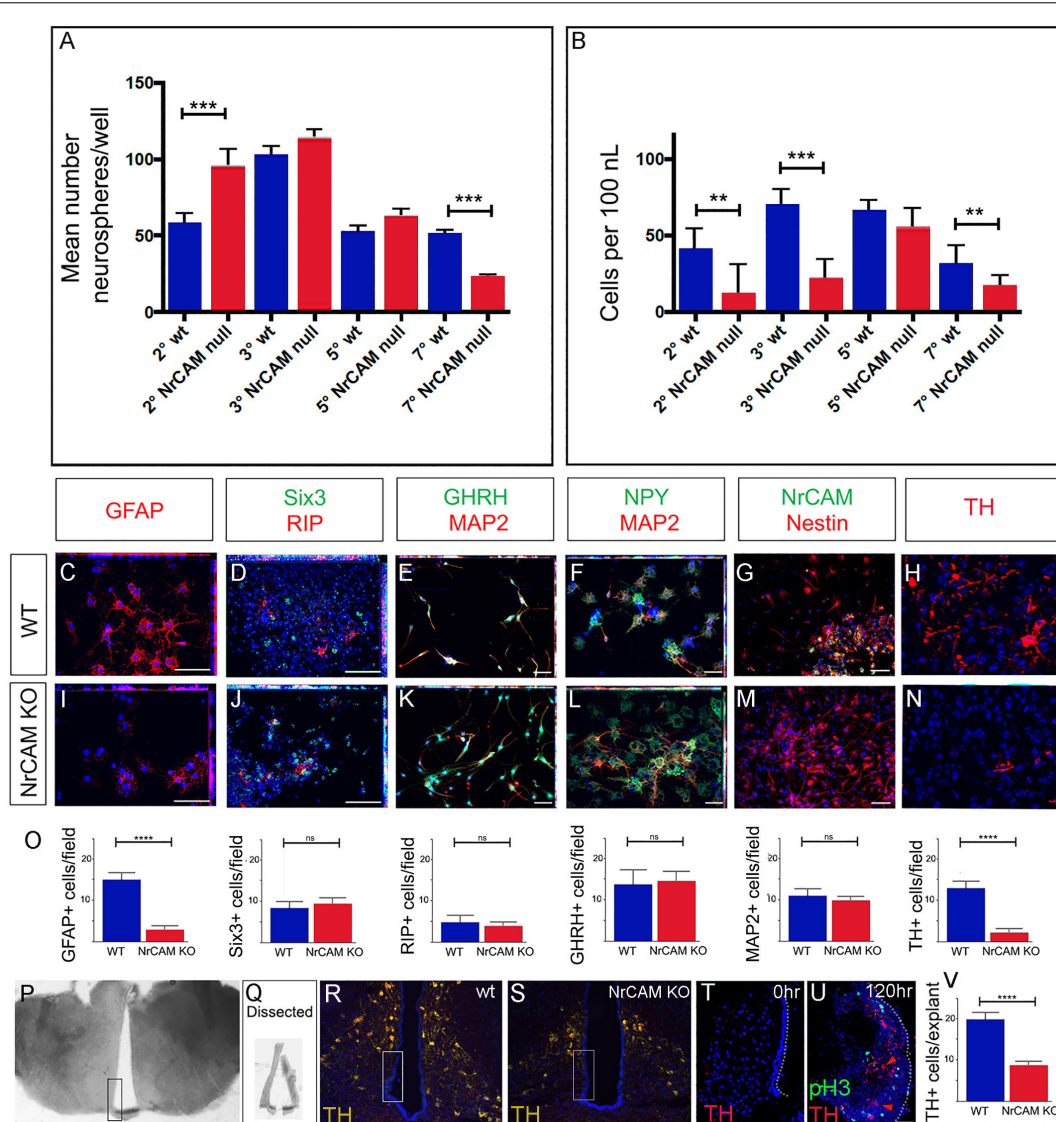
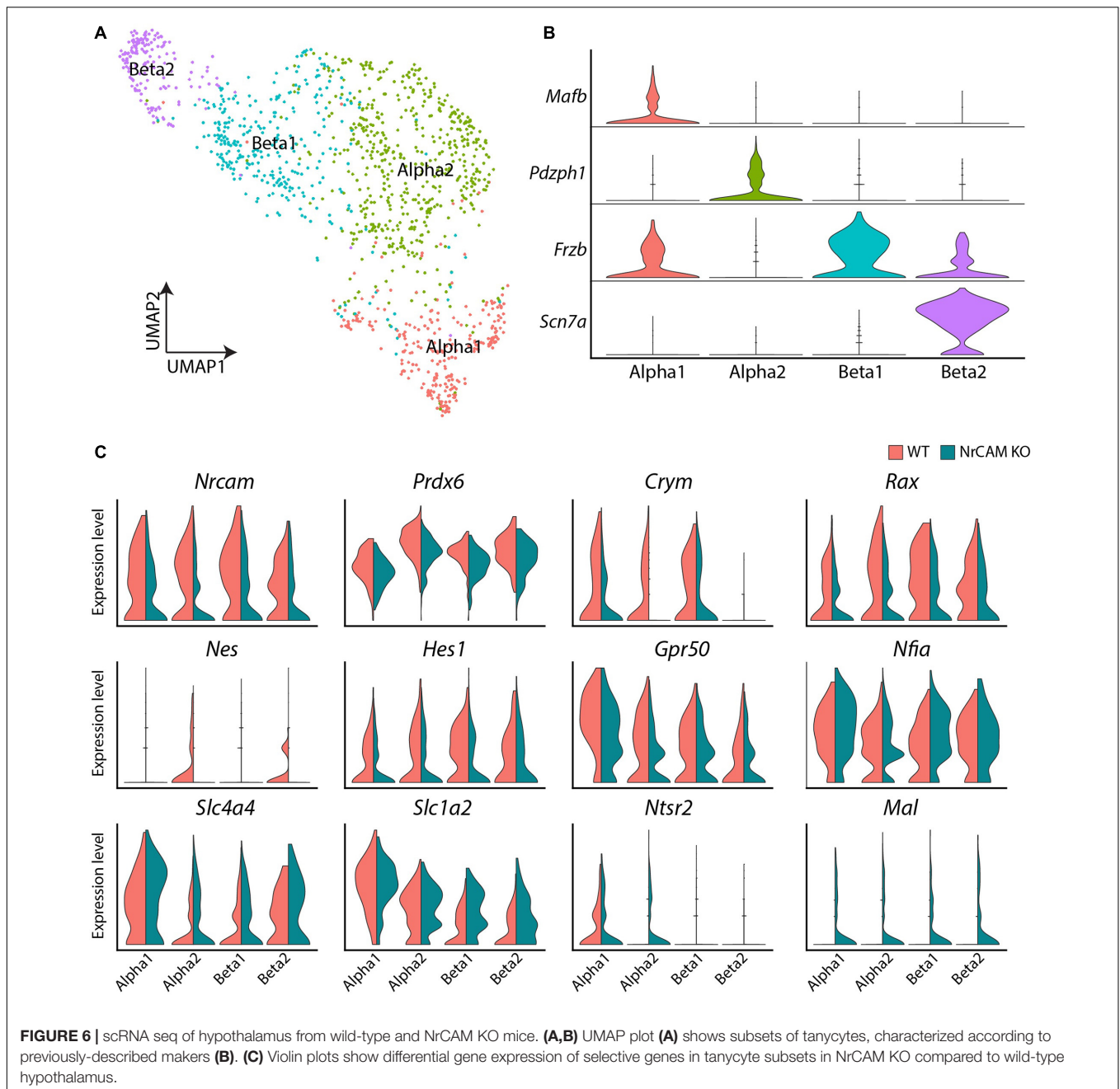


FIGURE 5 | Decreased proliferation/differentiation of NrCAM-derived VZ/SVZ tissues. **(A)** Average number neurospheres/well number in wild-type and NrCAM KO mice. The number of neurospheres from NrCAM null mice is significantly increased at passage 2 ($p = 0.0006$) and is significantly decreased at passage 7 ($p \leq 0.0001$). Error bars show SE ($n = 6-12$ wells; 3 mice each). **(B)** The number of cells per ml cultured from wild type and NrCAM KO mice (calculated by dissociation of neurospheres from 12 wells). Neurospheres from NrCAM KO have a reduced number of cells per ml than wild type at passage 2, 3 and 7. Error bars show SE. **(C-O)** Fields of view **(C-N)** of neurospheres from passage 6, subject to differentiation conditions and analyzed by immunohistochemistry after 7 days **(C-G, I-M)** or 14 days **(H, N)**. Neurospheres from wild-type **(C-H)** and NrCAM KO littermates **(I-N)** show a similar range of differentiated cells. Quantitative analyses **(O)** show significantly fewer GFAP-positive astrocytes (unpaired t -test, $p < 0.0001$) and significantly fewer TH-positive neurons (unpaired t -test, $p < 0.0001$) ($n = 5$ neurospheres analyzed from each of 3 replicates; 30 fields of view total). **(P-V)** Dissection and culture of 10 week hypothalamic tanycytes. **(P)** A 100 μm thick slice through the region of the ME. Boxed region shows dissected area. **(Q)** Examples of dissected hypothalamic VZ. **(R, S)** Boxed regions show approximate position of dissected VZ in wild-type and NrCAM KO mice. **(T)** Representative example of a 15 μm section through a VZ explant at $t = 0$ h, immunolabeled with anti-TH. No TH-positive cells are detected. **(U)** Representative example of a 15 μm section through a VZ explant at $t = 120$ h, immunolabeled with anti-TH and anti-phosphoH3. **(U)** Quantitative analyses show significantly fewer TH-positive neurons after culture of VZ explants from NrCAM KO mice (unpaired t -test, $p < 0.0001$) ($n = 10$ explants/genotype, from 3 mice). Bars show SE. Statistical significance denoted in charts by asterisks: ** $p < 0.01$, *** $p < 0.001$, **** $p < 0.0001$. Scale bars: 50 μm .

food intake (**Figures 8A,B**; two-way ANOVA time \times treatment interaction $p < 0.05$ and $p < 0.01$ respectively). Interestingly, in these animals, the respiratory exchange ratio (RER) was significantly reduced during the light phase (**Figure 8C**: two-way ANOVA time \times treatment interaction $p < 0.05$). Oxygen consumption and total activity were unaffected in NrCAM KO animals (**Figures 8D,E**).

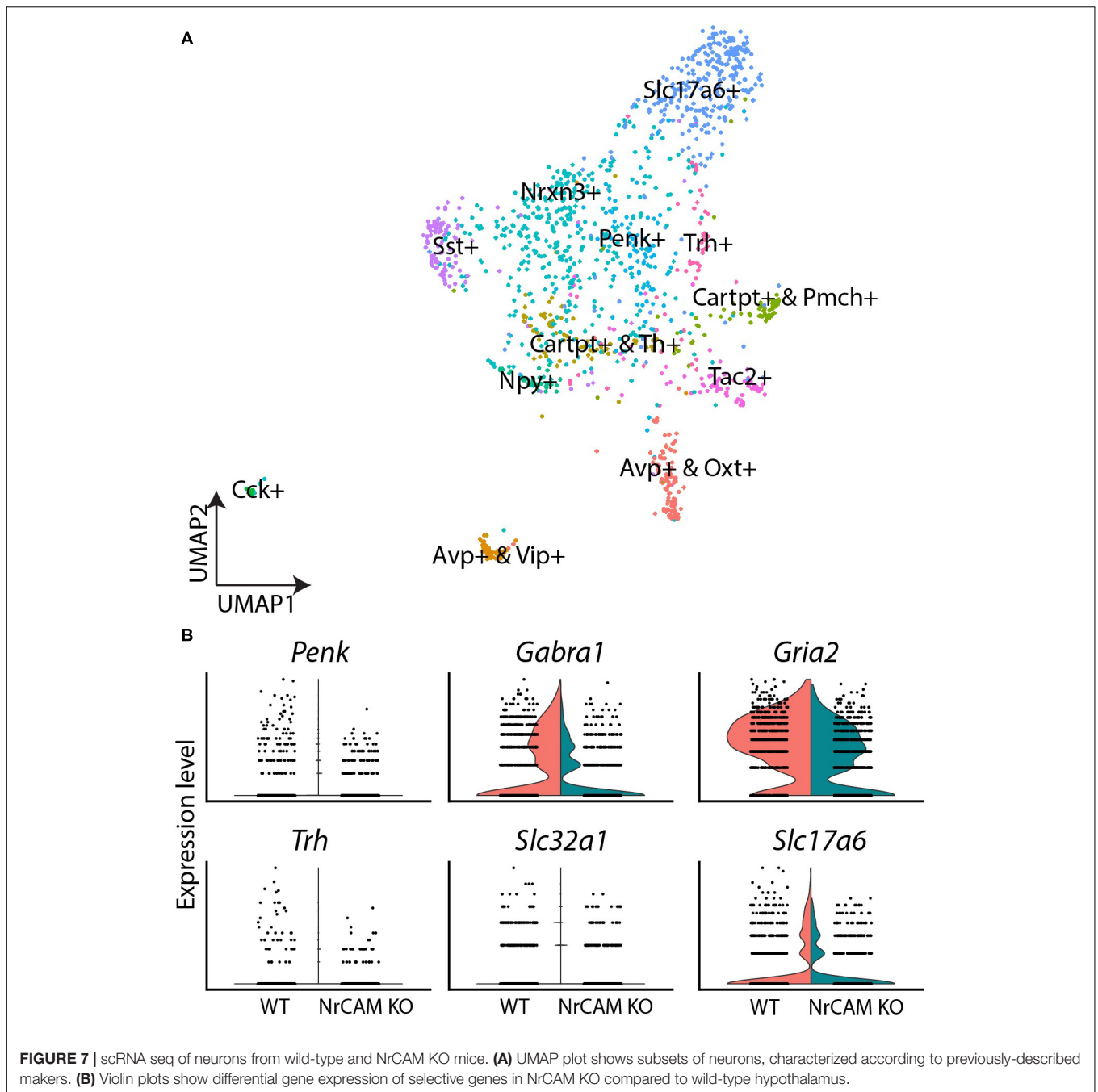
DISCUSSION

This study provides evidence that the neural cell adhesion molecule NrCAM regulates tanycytes that line the 3V of the hypothalamus. In wild-type mice, NrCAM is detected on hypothalamic embryonic radial glia and is then maintained at high levels on radial glia-derived tanycytes in the



postnatal/adult animal. NrCAM KO mice, in which *Nrcam* RNA is reduced and NrCAM protein cannot be detected, have significantly fewer tanyocytes than their wild-type siblings. Previous studies have suggested that tanyocytes are stem and progenitor cells within a hypothalamic stem cell niche (Robins et al., 2013; Yoo et al., 2021), and that *Rax*, *Lhx2* and *Fgf10* play ongoing roles in late embryonic/postnatal life to support tanyocyte differentiation and proliferation (Haan et al., 2013; Robins et al., 2013; Miranda-Angulo et al., 2014; Salvatierra et al., 2014). Our study adds to this, providing evidence that NrCAM supports cellular homeostasis within this niche.

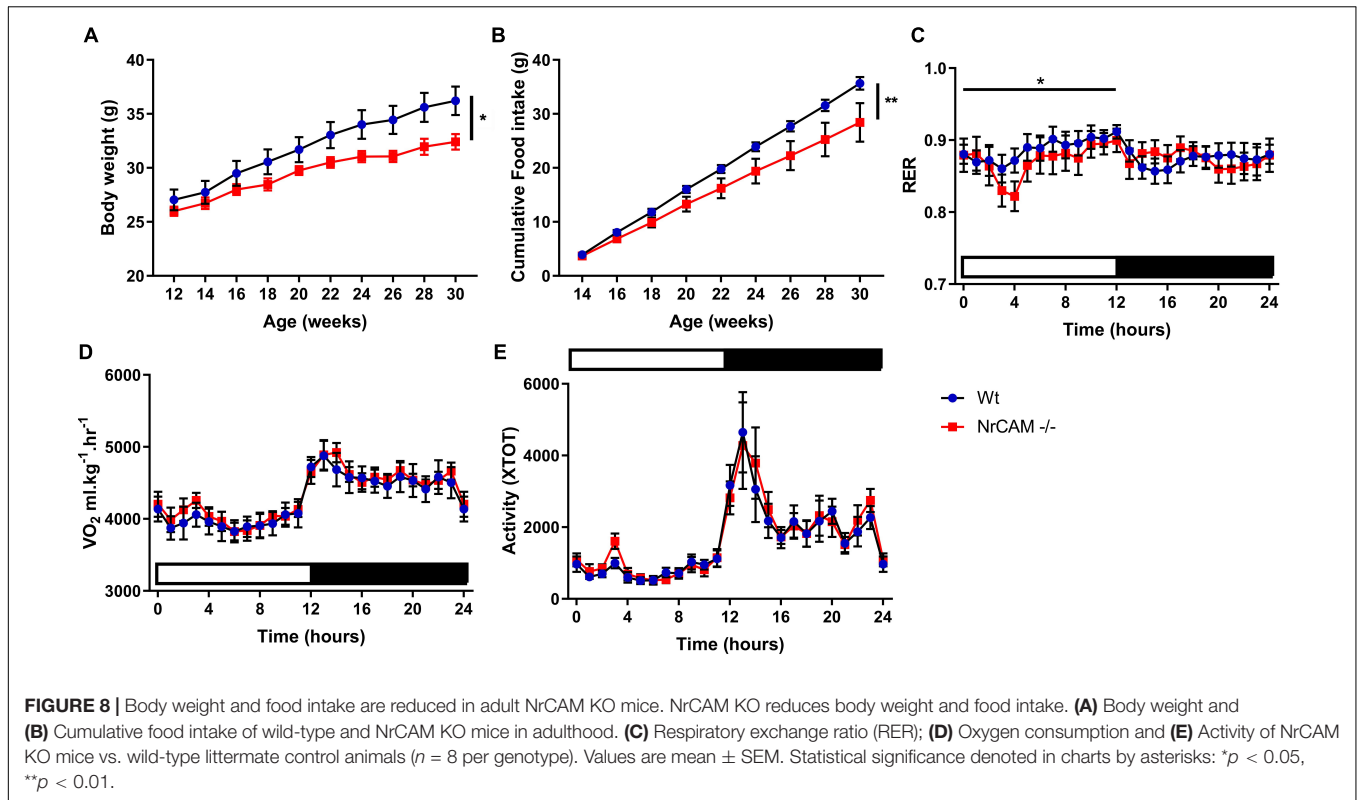
The loss of NrCAM does not appear to interfere with early hypothalamic specification or growth: at E16, hypothalamic length and morphology, and expression domains of the transcription factors *Rax* and *Six3*, and the signaling ligands, *Fgf10* and *Shh*—all of which regulate tuberal hypothalamic progenitor domains (Placzek et al., 2020)—are indistinguishable in WT and NrCAM KO siblings. Likewise, the transcription factor, *Lhx2*—also known to direct tanyocyte differentiation (Salvatierra et al., 2014)—and *Nestin* are indistinguishable at E16 in most of the hypothalamus in wild-type and NrCAM KO siblings. However, we detect a small but significant reduction in the density of *Lhx2* and *Nestin*-positive radial glial cells



in a limited spatial domain around the emerging ME. The reduction in radial glia in this region appears to prefigure a small but significant increase in embryonic TH-positive neurons in NrCAM mice compared to wild-type siblings—again, restricted to ME regions. The first manifestation of loss of NrCAM, therefore, appears to be a subtle imbalance, in late embryonic stages, in the numbers of radial glia and TH-positive Arc neurons.

By adulthood (8–10 weeks), there are significantly fewer tancytes throughout the hypothalamus in NrCAM mice compared to wild-type siblings. This is apparent through reduced numbers of Six3-positive VZ cells, a thinning of the VZ, reduced

density of Nestin- and GFAP-positive tancyte processes and a reduction in tancyte-enriched genes, including *Hes1*, *Rax* and *Lhx2* (Shimogori et al., 2010; Lee et al., 2012; Salvatierra et al., 2014). ScRNA seq analysis of the tancytic fraction demonstrates that the reduction in tancyte-enriched genes is accompanied by an increase in glial markers. At the same time, scRNA seq demonstrates a reduction—in the astrocyte fraction—of astrocyte-enriched genes. Previous genetic lineage-tracing studies have demonstrated that adult tancytes give rise to hypothalamic astrocytes (Lee et al., 2012; Haan et al., 2013; Robins et al., 2013; Yoo et al., 2021). Because NrCAM is expressed



in astrocytes, we cannot exclude that the reduction in astrocyte-enriched genes is a direct consequence of the loss of NrCAM in astrocytes. However, an alternate interpretation is that the reduction in astrocytes is, as least in part, a consequence of a reduction in astrocyte-generating tanycytes. Support for this idea comes through neurospherogenic assays: under differentiation conditions, neurospheres from NrCAM KO hypothalamic tissue generate smaller numbers of GFAP-positive astrocytes than do neurospheres from wild-type siblings. Potentially, tanycytes and hypothalamic astrocytes are transcriptionally similar cell types, whose balance is disrupted by loss of NrCAM. An intriguing possibility is that tanycytes and astrocytes are similar cell states, as is the case in other brain niches (Doetsch et al., 1999; Cebrian-Silla et al., 2021). scRNA seq show changes, in NrCAM KO tanycytes, in the expression of *Metr*, *Ndn* and *Ntsr1*—all previously shown to govern neural stem cell proliferation and/or the differentiation of neural stem cells to astrocytes (Nishino et al., 2004; Huang et al., 2013; Ando et al., 2019)—raising the possibility that these may be part of a regulatory network that governs tanycyte and astrocyte states in the hypothalamus. Future studies, using an inducible KO of NrCAM, are needed to better understand the role of NrCAM in cellular homeostasis, both in late embryonic life and in the adult.

Our analyses extend previous characterization of wild-type hypothalamic neurospheres (Robins et al., 2013) and reveals that, under non-differentiating conditions, they maintain expression of the regional stem/progenitor markers, *Nkx2-1* and *Six3*, and also express NrCAM. Hypothalamic neurospheres derived

from NrCAM KO mice maintain regional markers, but show decreased proliferation/ability to passage. The different behavior of neurospheres from NrCAM and wild-type mice indicates a direct role for NrCAM in tanycyte regulation. Intriguingly, the NrCAM KO neurospheres follow a culture pattern that is similar to progenitor-like tanycytes, rather than stem-like tanycytes (Robins et al., 2013)—an initial increase in neurosphere number, followed by a decrease and failure to culture beyond late passage. Thus, NrCAM KO may directly affect the behavior of stem-like tanycytes. Certainly in the intact NrCAM KO hypothalamus we detect a significant reduction in tanycytes in the region occupied by $\alpha 2$ (stem-like) tanycytes, as judged by the low numbers of GFAP-positive processes and *Lhx2*-positive nuclei. In other regions of the nervous system, NrCAM has been implicated in the control of progenitor cell proliferation. In the cerebellum, NrCAM was shown to be required to modulate granule neuron progenitor proliferation in response to SHH (Xenaki et al., 2011) and loss of NrCAM together with its sister protein L1CAM leads to severe cerebellar hypoplasia (Sakurai et al., 2001). More recently, NrCAM has been shown to be upregulated in androgen-treated proliferating neural stem cells (Quartier et al., 2018).

Numerous studies have shown that tanycytes can be stimulated to neurogenesis, but a key unknown question is whether tanycytes can give rise to hypothalamic neurons in the unchallenged animal. Our studies raise the possibility that tanycytes may generate TH-positive Arc neurons: we detect a small, but significant decrease in the adult, which contrasts with the increase in TH-positive neurons detected in the embryo. Further, we can detect the generation of TH-positive neurons,

both in differentiating neurospheres and in an acute assay that monitors the behavior of hypothalamic VZ cells. In each assay, significantly fewer TH-positive neurons are generated from NrCAM-KO tissue, compared to wild-type tissue. We did not, however, detect a decrease in *Th* mRNA in the scRNA seq analyses; potentially the lower numbers of TH-positive Arc neurons are masked by more abundant TH-positive neurons of the zona incerta, whose numbers are unaffected by loss of NrCAM. The scRNA-seq analysis does, however, show other subtle alterations in neuronal gene expression profiles, namely a reduction in GABAergic markers and *Trh*. Although we detect no NrCAM expression in neurons, the scRNA seq demonstrates neuronal expression of *NrCAM*, making it difficult to judge whether the alterations are a direct consequence of loss of NrCAM in neurons or an indirect effect due to a reduction in tanycytes.

The reduction in *Trh* expression in neurons, and reduction in tanycytic *Crym*—which encodes a thyroid hormone binding protein, *Gpr50*—is likewise involved in thyroid hormone metabolism, and *Ndn*, which encodes the Prader-Willi syndrome-deleted gene, *Necdin*, and modulates the thyroid axis (Hasegawa et al., 2012; Robins et al., 2013), raises the possibility that NrCAM KO animals may show alterations in metabolism. Indeed, from 8 weeks, NrCAM KO animals have lower body weight than wild-type littermate controls, and significantly reduced food intake. This subtle change appears to be a consequence of reduced food intake during the light phase, as the RER is significantly lower, suggesting increased fat oxidation. No change in energy expenditure or activity was apparent.

Finally, our systematic analysis demonstrates that as tanycytes develop from embryonic radial glia, they diversify along the A-P axis, and project, not only to the Arc and VMN but also to the periventricular nucleus (posterior part) (PVp). In contrast to tanycytes that project to the Arc and VMN, *Six3*, *Fgf10* and GFAP are either not detected or show weak expression in tanycytes that project to the PVp. Future studies are needed to determine the functional significance of this difference.

MATERIALS AND METHODS

Animals

For molecular and neurospherogenic assays, adult mice were taken at 8–12 weeks, and embryonic mice at E16. NrCAM knock-out (KO) (*Nrcam*^{tm1Gmt}/*Nrcam*^{tm1Gmt}) transgenic mice, described elsewhere (Sakurai et al., 2001). Wild type and NrCAM KO siblings were bred within an NrCAM[±] colony back-crossed to C57BL/6J^{OlaHsd} for > 10 generations. For molecular and neurospherogenic analyses, mice were kept in standard conditions for the duration of the study (18% protein rodent diet). Mice were housed in a centralized pathogen-free facility on a 12 h light/dark cycle, at 19–23°C with 55% (±10%) humidity and 15–20 air changes per hour. For adult physiological studies, mice were re-derived at the University of Nottingham. Climates at both facilities were similar. All studies and procedures were conducted according to the

United Kingdom Animals (Scientific Procedures) Act 1986/EU Directive 2010/63/EU, and were approved by the University of Sheffield Local Ethical Review committee (License 40/3742 to AF) and the University of Nottingham Local Ethical Review committee (License PFBB5B31F to FE).

Tissue Processing, Immunohistochemistry and *in situ* Hybridization

Adult mice were anaesthetized by inhalation of isoflurane anesthetic (B506; Abbott) before transcardial perfusion with 4% paraformaldehyde in 0.12 M phosphate buffer (4% PFA PB). Brains were dissected in ice cold Leibovitz's 15 (L-15) media (11415-049; GIBCO), postfixed in 4% PFA PB at 4°C overnight, then transferred to 30% sucrose (S0389; Sigma), rocking at 4°C for 2–3 days until they sank. Prior to mounting, the anterior forebrain, hindbrain, and cerebellum were removed. The remaining medial portion of the brain containing the hypothalamus was orientated in OCT (361603E; VWR International) and frozen on dry ice before storage at –80°C.

Embryonic mice were collected in accordance with Schedule 1 methodology: pregnant dams were terminally anaesthetized as above and subjected to cervical dislocation. Embryos were removed on ice and decapitated. Intact skulls were fixed in 4% PFA PB overnight at 4°C, brains removed and postfixed in 4% PFA PB for a further 3 h at 4°C before transfer to 30% sucrose, rocking overnight. Brains were embedded in OCT, frozen on dry ice and transferred to –80°C for storage.

Sequential serial 15 µm-thick coronal sections using a cryostat (Leica Biosystems). For adults, sections were taken over a ~1,500 µm length, covering Allen Brain Atlas sections 65–80. For embryos, sections were taken over a ~700 µm length, centered around the visibly obvious median eminence. For immunohistochemistry, serial floating sections were collected in PBS. For *in situ* hybridization, serial sections were collected directly onto Superfrost Plus slides (Fisher Scientific).

For immunohistochemical analysis, adult samples were rinsed in PBS, then incubated in Citrate Buffer (10 mM Citric Acid (277804I; BDH), 0.05% Tween 20 (P9416; Sigma), pH 6.0) at 90°C for 1 h for antigen retrieval. Sections were cooled for 20 min, rinsed in PBS and blocked in PBS with 0.5% TritonX-100 (T8787; Sigma) and 5% heat-inactivated goat serum (16210-072; GIBCO). Embryonic samples were rinsed in PBS and directly blocked in PBS with 0.1% TritonX-100 and 1% heat-inactivated goat serum. After a 1 h block at room temperature, samples were incubated with primary antibody diluted in blocking buffer at 4°C overnight, rinsed in PBS, then incubated with secondary antibody in blocking buffer for 1 h at room temperature. Negative controls were performed in an identical manner, without incubation with primary antibody. For adult tissue, DAPI (D9542-10MG; Sigma) was added at 100 ng/mL to the secondary antibody solution. Floating sections were mounted onto Superfrost Plus slides by careful manipulation with forceps and fine paintbrushes in a small quantity of 0.5X PBS. Excess liquid was removed from slides and sections coverslipped in Vectashield antifade mounting

medium (#H-1200, Vector Laboratories) before imaging on a Zeiss Axioimager Z1 with Apotome2 attachment and viewed in the Zeiss Zen 2 image acquisition software. Views show maximum intensity projections.

Antibodies used were as follows: mouse anti-GFAP (1:50, cat no. 556330, BD Pharmingen); mouse anti-MAP2 (1:1,000, cat no. M9942, Sigma-Aldrich); mouse anti-Nestin (1:200, cat no. Ab6142, Abcam); rabbit anti-NPY (1:1,000, cat no. 22940, Immunostar); rabbit anti-NrCAM (1:1,000, gift of Lustig et al., 2001); rabbit anti-Nkx2.1 (custom antibody, Ohyama et al., 2005); rabbit anti-phosphoH3 (1:1,000, cat no. 06-570, Millipore); anti-mouse RIP [1:10 cat no. AB531796, Developmental Studies Hybridoma Bank (DSHB)]; anti-rabbit Six3 (1:10,000, Eurogentec custom antibody; sequence RLQ-HQA-IGP-SGM-RSL-AEP-GC); mouse anti-Slc1a3 (Glast, 1:1,000, Ab 49643, Abcam); anti-rabbit Sox2 (1:200, cat no. Ab97959 Abcam); anti-rabbit TH (1:1,000, cat no. Ab152, EMD Millipore); mouse anti-Pax6 (1:50, DSHB); rabbit anti-GHRH (1:600, AB1715, Chemicon); mouse anti-Vimentin (1:200, Sigma); mouse anti-Ki67 (1:500, Ab15580, Abcam); mouse anti-Nkx6.1 (1:50, F55A10, DSHB); goat anti-rabbit Alexa 488 (1:100, cat no. A11034, Molecular Probes); goat anti-rabbit Alexa 594 (1:500, cat no. A11012, Molecular Probes); goat anti-mouse IgG Alexa 488 (1:500, cat no. A11001, Molecular Probes); goat anti-mouse IgG Alexa 594 (1:500, cat no. A11005, Molecular Probes).

Chromogenic *in situ* hybridization was performed as previously described (Miranda-Angulo et al., 2014). Briefly, 15 μm coronal sections were fixed with 4% paraformaldehyde, permeabilized in PBS with 0.1% TritonX-100, then acetylated [1.3% triethanolamine (90279; Sigma), 2.1 M HCl (H/1150/PB17; Fisher Scientific) and 0.25% acetic anhydride (added last) (A6404; Sigma)]. Sections were hybridized with anti-sense, or as negative control, sense digoxigenin-labeled probes at 68°C overnight. Unbound probes were washed out and sections were blocked with sheep serum followed by incubation with anti-digoxigenin antibodies conjugated to alkaline phosphatase (1:5,000) overnight at 4°C. Nitro-blue tetrazolium (NBT) and 5-bromo, 4-chloro, 3-indolylphosphate (BCIP) were used as chromogenic substrates of alkaline phosphatase. Color development was continued for the same amount of time for wild-type and NrCAM KO sections.

Neurospherogenic Assays and Organotypic Cultures

Animals were sacrificed using a lethal dose of isoflurane anesthetic and cervical dislocation. Brains were removed into ice-cold L-15, and the hypothalamus was manually isolated.

Neurospherogenic assays were performed as previously described (Robins et al., 2013). Briefly, hypothalamic regions close to the VZ were isolated from adjacent parenchyma using tungsten needles, minced and enzymatically dissociated using TrypLE enzyme solution (12604013, Life Technologies) for 20 min at 37°C, then mechanically dissociated by trituration to single-cell suspension using 25-gauge and 30-gauge needles. Cells were plated in Corning Costar Ultra-Low attachment 24 well plates (3473 SLS) in DMEM:F12 (21331; GIBCO) supplemented

with 100 U/mL penicillin/streptomycin (11578876; Fisher Scientific), 2 mM L-Glutamine (25030024; GIBCO), 1X B27 (17504-044; Life Technologies), 5 $\mu\text{g}/\text{ml}$ heparin, 10 μM transferrin (T0665; Sigma), 20 nM progesterone (P7556; Sigma), 30 nM selenite (S5261; Sigma), 100 μM putrescine (P5780; Sigma), 50 ng/mL IGF-1 (I8779-50UG; Sigma), 20 ng/mL bFGF (13256029; Life Technologies), and 20 ng/mL EGF (PHG0314; Life Technologies). Primary neurosphere cultures were maintained at 37°C and 5% CO₂ and assessed 7 days after plating. Neurospheres were passaged by incubating for 20 min in TrypLE solution, before dissociating and plating as per the original conditions. From first passage onward, neurospheres were fed every other day. Neurospheres were differentiated in Nunc Lab-Tek 8-well Permax chamber slides (C7182; Sigma) coated with poly-D-lysine (P1024; Sigma) for 1 h and fibronectin (10042682; Fisher Scientific) for 4 h. Differentiation media was made to the same specification as neurosphere culture media but without IGF-1, EGF, reduced bFGF (10 ng/mL), and with B27 supplement replaced with B27 minus insulin (A1895601; Thermo Fisher). One neurosphere was added to each well and cultured for 7 or 14 days as specified. Differentiation cultures were fed every 2 days, before fixation and processing.

For organotypic assays, the hypothalamus was mounted coronally on a McIlwain tissue chopper and 100 μm -thick slices were obtained. Electrolytically-sharpened tungsten needles were used to isolate the VZ from tuberal slices. Explants were embedded in collagen, as described elsewhere (Placzek and Dale, 1999) and cultured in 0.5 mL Opti-MEM (31985070; Fisher Scientific) with 100 U/mL penicillin/streptomycin (11578876; Fisher Scientific), 2 mM L-Glutamine (25030024; GIBCO), and 4% FBS (10042682; Fisher Scientific) (Placzek et al., 1993) supplemented with 3 nM Shh (1845-SH; R&D Systems), as used in Ohyama et al. (2005) to promote hypothalamic neuron differentiation from prospective hypothalamic tissue. Following culture, explants were fixed in 4% PFA PB for 2 h at 4°C, transferred to 30% sucrose overnight, then embedded in OCT for cryostat sectioning at 15 μm .

Tanycyte Process and Cell Counts

All counts were performed along the sides of the VZ, in the regions covered by $\alpha 2$ - and $\beta 1$ -tanycytes. Nestin-positive process counts and TH-positive cell counts were performed blindly, on every alternate section (~30 sections in adult covering sections every 30 μm between Bregma -0.9 to -2.2/every 30 μm over ABRA sections 67-77); 15 sections in embryo, centered around ME); GFAP-positive process counts, Six3-positive and Lhx2-positive cell counts and DAPI-positive measurements were performed on every 5th section over the length of the ME (ABRA sections 69-73); centered around ME in embryo. All counts were analyzed independently by a second individual. Processes were marked by eye with the ImageJ multipoint tool, where they first extend into the SVZ from the VZ. Process numbers were normalized to length, to obtain a measure of process density (processes per μm). All values are expressed as means \pm SD.

For neurospherogenic assays, cells were counted in 20x random fields; in organotypic assays, cells were counted from each 15 μm section taken through the entire explant.

Quantification of Chromogenic ISH Signal

Quantification of *Rax*, *Fgf10*, and *Shh*-expression in the VZ was performed blindly, on every 5th section (adult regions sampled over ABRA sections 67–77; embryonic sections sampled around ME). Length measurements were collected using the ImageJ segmented line tool. Signal intensity was obtained from a one-pixel line profile through the chromogenically labeled domain, and the mean gray value was measured. Intensity was normalized to a line profile through the adjacent non-labeled parenchyma. Isolated *Shh* or *Rax*-positive cells were quantified using the ImageJ multi-point tool.

scRNA seq Analysis

Hypothalamic tissue was manually dissected and transferred to Hibernate E medium (Cat No. HE500, BrainBits LLC). Tissue was enzymatically digested using Papain (2 mg/ml, Cat No. LS003119, Worthington Chemicals), and cells dissociated into single cells using fire-polished glass pipettes. Papain was neutralized with Hibernate-A medium with B27 and GlutaMAX (Kim et al., 2020). Cells were pelleted at 500 *g* at 4°C, washed twice in 1 ml cold 1 × PBS, and then resuspended in 200 μl chilled 1 × PBS by gentle pipetting. Cells were then fixed with 800 μl cold 100% methanol as previously described (Alles et al., 2017). Cells were stored at –80°C until scRNA-Seq, then re-hydrated as previously described (Alles et al., 2017). Briefly, cells were washed twice (3,000 × *g* for 5 min at 4°C) and resuspended in RNase-free PBS with 1% BSA and 0.5 U/μl RNase inhibitor (Cat. N2615, Promega). Cells were then used for the 10x Genomics Chromium Single Cell System (10x Genomics, CA, United States) using V3.0 chemistry per manufacturer's instruction, loading between 8,000 and 12,000 cells per run. Libraries were sequenced on Illumina NextSeq 500 with ~400 million reads per library. Sequenced files were processed through the Cell Ranger pipeline (v.3.10, 10x Genomics), and scRNA-Seq analysis was conducted as described previously (Kim et al., 2020).

Physiological Measurements

Bodyweight and food intake in the home cage were measured at 2-week intervals. At approximately 2, 6 and 9 months of age energy expenditure parameters and feeding behavior were measured using a comprehensive lab animal monitoring system (CLAMS: Linton Instrumentation, Linton, United Kingdom, and Columbus Instruments, Columbus, OH, United States). This is comprised of 8 chambers in which mice were individually housed, with water bottles and food hoppers located at the center of each chamber. Metabolic activity was measured in a variety of ways including oxygen consumption (VO₂) and respiratory exchange ratio (RER; CO₂ production/VO₂). Locomotor activity was measured *via* infrared beams that cross each cage, monitoring movement along the x, y, and z axes. Locomotor activity was calculated as the number of infrared beam breaks recorded in 9-min time intervals. Feeding behavior of the animals was also monitored to establish total food intake and parameters such as meal size and duration and timing of each feeding bout. The diet used for this study consisted of standard laboratory

chow comprising 19% extruded protein and 9% fat (Teklad 2019, Harlan, United Kingdom). All raw metabolic data were recorded in 9-min intervals and collected from the CLAMS using OxyMax software (v4.2, Columbus Instruments). Male mice (8 NrCAM KO, 8 wild-type littermates) were placed in the CLAMS at approximately 2 months of age (mean = 8.6 weeks, range: 7.9–10.9 weeks), 6 months of age (mean = 26.3 weeks, range: 24.9–28.9 weeks), and 9 months of age (mean = 36.3 weeks, range: 31.0–39.4 weeks). The mice were maintained on a 12 h light/dark cycle, and were initially placed in the metabolic chambers during the light phase, and maintained for 48 h. Data for the second 24 h period were analyzed to allow the mice time to acclimatize to the chambers.

Statistical Analyses

Analyses of studies with two groups (genotypes) were performed through two-tailed Student's *t*-test (Microsoft Excel). Chromogenic signal measurements were statistically analyzed in GraphPad Prism 7.04 using the Wilcoxon matched-pairs signed-rank test. Descriptive statistics (means ± SEM) were generated using GraphPad Prism (version 9.0, San Diego, CA, United States). Data were analyzed using two-way ANOVA. No animals were excluded from the analyses. Statistical significance was considered at *p* < 0.05.

DATA AVAILABILITY STATEMENT

All relevant data are within the manuscript and its supporting information files. All sequencing data is publicly available on GEO: <https://www.ncbi.nlm.nih.gov/geo/>, GSE192766.

ETHICS STATEMENT

The animal study was reviewed and approved by University of Sheffield Local Ethical Review committee (License 40/3742 to AF) and the University of Nottingham Local Ethical Review committee (License PFBB5B31F to FE).

AUTHOR CONTRIBUTIONS

AF and MP conceived the study. AM, KC, SaB, and IS performed *in vivo* characterization. SaB, KC, AM, SR, and MP performed neurospherogenic and organotypic assays. SeB and DK generated and analyzed scRNA-Seq data. IS, JL, GD, CM, MT, and FE performed physiological assays. MP drafted the manuscript. SeB, AF, AM, DK, KC, IS, SaB, JL, and FE edited the manuscript. All authors contributed to the article and approved the submitted version.

FUNDING

This work was supported by the Wellcome Trust (212247/Z/18/Z) to MP, NIH (R01DK108230 and

R01MH126676) to SeB, the Maryland Stem Cell Research Fund (2019-MSCRFF-5124) to DK, and British Society for Neuroscience to JL.

ACKNOWLEDGMENTS

We would like to thank Transcriptomics and Deep Sequencing Core (Johns Hopkins) for sequencing of scRNA-Seq libraries.

SUPPLEMENTARY MATERIAL

The Supplementary Material for this article can be found online at: <https://www.frontiersin.org/articles/10.3389/fnins.2022.832961/full#supplementary-material>

Supplementary Figure 1 | Medial-most cells in the tuberal hypothalamus express *Shh*. (A–D') Representative examples from consecutive serial adjacent coronal sections (same sample as shown in **Figures 1M–T'**) across the AME, ME, PME and posterior tanycyte-rich hypothalamus, analyzed for expression of *Shh*. Boxed regions in panels (A–D) shown at high power in panels (A'–D'). Arrowheads in panels (B',C') point to *Shh*-expressing VZ cells ($n = 3$ mice; images from a single mouse). Scale bar: 100 μm .

Supplementary Figure 2 | Selective expression of regional markers in neurospheres cultured from different regions of the CNS. (A,D,G) Coronal/transverse sections through 8–10 week adult tuberal hypothalamus (A), lateral ventricle of the brain (D) and spinal cord (G), after *in situ* hybridization to detect *Six3*. Boxed regions shown in high power in panels (A',D',G'). Arrow in panel (D') points to weak expression of *Six3* in the subventricular zone (SVZ). Dotted outline in panel (G') shows ependymal region ($n = 4$ mice). (B,C,E,F,H,I) Representative examples of sections through neurospheres cultured under non-differentiated conditions, analyzed by *in situ* hybridization for *Six3* expression (2 from each region to show range; $n = 10$ neurospheres from each of 3 replicates). Only hypothalamic neurospheres show strong *Six3* expression. (J–U) Representative examples of sections from neurospheres from hypothalamus, SVZ of the lateral ventricle, and spinal cord ependymal region, cultured under non-differentiated conditions, analyzed by immunohistochemistry. Neurospheres from all regions express the pan-neural stem cell markers, Sox2 and Vimentin, and

proliferate (Ki67-positive), but only those from spinal regions express Nkx6-1 ($n = 5$ neurospheres analyzed from each of 3 replicates; 30 fields of view total).

Supplementary Figure 3 | Comparative analyses in wild-type and NrCAM KO mice. (A–J) Coronal sections through wild-type (A,C,E,F,I) or NrCAM KO (B,D,G,H,J) mice. Panels (A–D) show sections at level of ME, immunolabeled with anti-NrCAM Ab ($n = 5$ mice/genotype) or anti-GnRH Ab ($n = 3$ mice/genotype). Panels (E–H) show serial coronal sections through AME, ME and posterior regions of the hypothalamus, analyzed by immunohistochemistry to detect NPY or by *in situ* hybridization to detect *Shh* ($n = 3$ mice each/genotype). Panels (I,J) show sections at the level of the AME, showing the dorsal zona incerta (A13) TH⁺ population ($n = 3$ mice/genotype). Inset in panel (J): Quantification of TH⁺ positive A13 cells (same 3 pairs of wild-type and NrCAM KO adult mice as shown in **Figures 3I,J,U,V**). Each icon represents a single measurement. Bars show 1 SD either side of the mean value. Analysis by unpaired *t*-test showed no significant difference of TH⁺ cells in dorsal AME Zona Incerta (A13) population between wild type and NrCAM KO adult mice ($p = 0.2543$). Arrowheads in panels (F',G') point to Shh midline cells. Scale bars: 100 μm .

Supplementary Figure 4 | Tanycyte progenitor markers at E16. (A–E) Representative serial coronal sections through AME, ME and posterior regions of the hypothalamus of a wild-type (A,B,D) or NrCAM KO mouse (C,E), analyzed by immunohistochemistry to detect NrCAM and Nestin (A) or by *in situ* hybridization to detect *Shh* and *Fgf10*. $n = 3$ mice/condition. Scale bars: 100 μm .

Supplementary Figure 5 | scRNA seq analysis of the hypothalamus. (A) UMAP plots showing detected cluster. (B) Violin plots showing *Nrcam* expression across cell types.

Supplementary Figure 6 | scRNA seq of astrocytes from wild-type and NrCAM KO mice. Violin plots show differential gene expression of selective genes in astrocytes from NrCAM KO compared to wild-type hypothalamus.

Supplementary Figure 7 | Body weight and food intake in newborn-juvenile NrCAM KO and wild-type mice. (A) Body weight in 3 pups of each genotype; (B) average food intake of wild-type and NrCAM KO mice at 5 and 6 weeks ($n = 6$ per genotype). Values are mean \pm SEM. Red—NrCAM KO; black—wild-type.

Supplementary Table 1 | Differential gene expression as measured by scRNA-Seq in tanycytes across genotype.

Supplementary Table 2 | Differential gene expression as measured by scRNA-Seq in astrocytes across genotype.

Supplementary Table 3 | Differential gene expression as measured by scRNA-Seq in neurons across genotype.

REFERENCES

- Alles, J., Karaikos, N., Praktinjo, S. D., Grosswendt, S., Wahle, P., Ruffault, P.-L., et al. (2017). Cell fixation and preservation for droplet-based single-cell transcriptomics. *BMC Biol.* 15:44. doi: 10.1186/s12915-017-0383-5
- Ando, T., Kato, R., and Honda, H. (2019). Identification of an early cell fate regulator by detecting dynamics in transcriptional heterogeneity and co-regulation during astrocyte differentiation. *NPJ Syst. Biol. Appl.* 5:18. doi: 10.1038/s41540-019-0095-2
- Bai, G., Sheng, N., Xie, Z., Bian, W., Yokota, Y., Benezra, R., et al. (2007). Id sustains Hes1 expression to inhibit precocious neurogenesis by releasing negative autoregulation of Hes1. *Dev. Cell* 13, 283–297. doi: 10.1016/j.devcel.2007.05.014
- Bechtold, D. A., Sidibe, A., Saer, B. R. C., Li, J., Hand, L. E., Ivanova, E. A., et al. (2012). A role for the melatonin-related receptor GPR50 in leptin signaling, adaptive thermogenesis, and torpor. *Curr. Biol.* 22, 70–77. doi: 10.1016/j.cub.2011.11.043
- Bjornsson, C. S., Apostolopoulou, M., Tian, Y., and Temple, S. (2015). It takes a village: constructing the neurogenic niche. *Dev. Cell* 32, 435–446. doi: 10.1016/j.devcel.2015.01.010
- Bosze, B., Moon, M.-S., Kageyama, R., and Brown, N. L. (2020). Simultaneous requirements for Hes1 in retinal neurogenesis and optic cup–stalk boundary maintenance. *J. Neurosci.* 40, 1501–1513. doi: 10.1523/jneurosci.2327-19.2020
- Cebrian-Silla, A., Nascimento, M. A., Redmond, S. A., Mansky, B., Wu, D., Obernier, K., et al. (2021). Single-cell analysis of the ventricular-subventricular zone reveals signatures of dorsal and ventral adult neurogenesis. *eLife* 10:e67436. doi: 10.7554/eLife.67436
- Chan, J. Y., Ong, C. W., and Salto-Tellez, M. (2011). Overexpression of neurone glial-related cell adhesion molecule is an independent predictor of poor prognosis in advanced colorectal cancer. *Cancer Sci.* 102, 1855–1861. doi: 10.1111/j.1349-7006.2011.02021.x
- Chen, S., Lewallen, M., and Xie, T. (2013). Adhesion in the stem cell niche: biological roles and regulation. *Development* 140, 255–265. doi: 10.1242/dev.083139
- Conacci-Sorrell, M., Kaplan, A., Raveh, S., Gavert, N., Sakurai, T., and Ben-Ze'ev, A. (2005). The shed ectodomain of Nr-CAM stimulates cell proliferation and motility, and confers cell transformation. *Cancer Res.* 65, 11605–11612. doi: 10.1158/0008-5472.CAN-05-2647
- Conacci-Sorrell, M. E., Ben-Yedidia, T., Shtutman, M., Feinstein, E., Einat, P., and Ben-Ze'ev, A. (2002). Nr-CAM is a target gene of the beta-catenin/LEF-1 pathway in melanoma and colon cancer and its expression enhances motility and confers tumorigenesis. *Genes Dev.* 16, 2058–2072. doi: 10.1101/gad.227502
- Doetsch, F., Caillé, I., Lim, D. A., García-Verdugo, J. M., and Alvarez-Buylla, A. (1999). Subventricular zone astrocytes are neural stem cells in the adult mammalian brain. *Cell* 97, 703–716. doi: 10.1016/s0092-8674(00)80783-7

- Edwards, M. A., Yamamoto, M., and Caviness, V. S. Jr. (1990). Organization of radial glia and related cells in the developing murine CNS. An analysis based upon a new monoclonal antibody marker. *Neuroscience* 36, 121–144. doi: 10.1016/0306-4522(90)90356-9
- Farkas, E., Varga, E., Kovács, B., Szilvássy-Szabó, A., Cote-Vélez, A., Péterfi, Z., et al. (2020). A glial-neuronal circuit in the median eminence regulates thyrotropin-releasing hormone-release via the endocannabinoid system. *iScience* 23:100921. doi: 10.1016/j.isci.2020.100921
- Gennarini, G., Bizzoca, A., Picocci, S., Puzzo, D., Corsi, P., and Furley, A. J. W. (2017). The role of Gpi-anchored axonal glycoproteins in neural development and neurological disorders. *Mol. Cell. Neurosci.* 81, 49–63. doi: 10.1016/j.mcn.2016.11.006
- Haan, N., Goodman, T., Najdi-Samiei, A., Stratford, C. M., Rice, R., El Agha, E., et al. (2013). Fgf10-expressing tanycytes add new neurons to the appetite/energy-balance regulating centers of the postnatal and adult hypothalamus. *J. Neurosci.* 33, 6170–6180. doi: 10.1523/JNEUROSCI.2437-12.2013
- Hasegawa, K., Kawahara, T., Fujiwara, K., Shimpuku, M., Sasaki, T., Kitamura, T., et al. (2012). Necdin controls Foxo1 acetylation in hypothalamic arcuate neurons to modulate the thyroid axis. *J. Neurosci.* 32, 5562–5572. doi: 10.1523/JNEUROSCI.0142-12.2012
- Heyden, A., Angenstein, F., Sallaz, M., Seidenbecher, C., and Montag, D. (2008). Abnormal axonal guidance and brain anatomy in mouse mutants for the cell recognition molecules close homolog of L1 and NgCAM-related cell adhesion molecule. *Neuroscience* 155, 221–233. doi: 10.1016/j.neuroscience.2008.04.080
- Hu, X.-L., Chen, G., Zhang, S., Zheng, J., Wu, J., Bai, Q.-R., et al. (2017). Persistent expression of VCAM1 in radial glial cells is required for the embryonic origin of postnatal neural stem cells. *Neuron* 95, 309.e6–325.e6. doi: 10.1016/j.neuron.2017.06.047
- Huang, Z., Fujiwara, K., Minamide, R., Hasegawa, K., and Yoshikawa, K. (2013). Necdin controls proliferation and apoptosis of embryonic neural stem cells in an oxygen tension-dependent manner. *J. Neurosci.* 33, 10362–10373. doi: 10.1523/JNEUROSCI.5682-12.2013
- Hynes, R. O. (2002). Integrins: bidirectional, allosteric signaling machines. *Cell* 110, 673–687. doi: 10.1016/s0092-8674(02)00971-6
- Ishiguro, H., Hall, F. S., Horiuchi, Y., Sakurai, T., Hishimoto, A., Grumet, M., et al. (2014). NrCAM-regulating neural systems and addiction-related behaviors. *Addict. Biol.* 19, 343–353. doi: 10.1111/j.1369-1600.2012.00469.x
- Ishiguro, H., Liu, Q.-R., Gong, J.-P., Hall, F. S., Ujike, H., Morales, M., et al. (2006). NrCAM in addiction vulnerability: positional cloning, drug-regulation, haplotype-specific expression, and altered drug reward in knockout mice. *Neuropsychopharmacology* 31, 572–584. doi: 10.1038/sj.npp.1300855
- Ishiguro, H., Miyake, K., Tabata, K., Mochizuki, C., Sakurai, T., and Onaivi, E. S. (2019). Neuronal cell adhesion molecule regulating neural systems underlying addiction. *Neuropsychopharmacol. Rep.* 39, 10–16. doi: 10.1002/npr.2.12038
- Kano, M., Suga, H., Ishihara, T., Sakakibara, M., Soen, M., Yamada, T., et al. (2019). Tanycyte-like cells derived from mouse embryonic stem culture show hypothalamic neural stem/progenitor cell functions. *Endocrinology* 160, 1701–1718. doi: 10.1210/en.2019-00105
- Kim, D. W., Washington, P. W., Wang, Z. Q., Lin, S. H., Sun, C., Ismail, B. T., et al. (2020). The cellular and molecular landscape of hypothalamic patterning and differentiation from embryonic to late postnatal development. *Nat. Commun.* 11:4360.
- Kinney, C. J., and Bloch, R. J. (2021). μ -Crystallin: a thyroid hormone binding protein. *Endocr. Regul.* 55, 89–102.
- Lazutkaite, G., Soldà, A., Lossow, K., Meyerhof, W., and Dale, N. (2017). Amino acid sensing in hypothalamic tanycytes via umami taste receptors. *Mol. Metab.* 6, 1480–1492. doi: 10.1016/j.molmet.2017.08.015
- Lechan, R. M., and Toni, R. (2016). “Functional anatomy of the hypothalamus and pituitary,” in *Endotext*, eds K. R. Feingold, B. Anawalt, A. Boyce, G. Chrousos, W. W. de Herder, K. Dhatriya, et al. (South Dartmouth, MA: MDText.com, Inc.).
- Lee, D. A., Bedont, J. L., Pak, T., Wang, H., Song, J., Miranda-Angulo, A., et al. (2012). Tanycytes of the hypothalamic median eminence form a diet-responsive neurogenic niche. *Nat. Neurosci.* 15, 700–702. doi: 10.1038/nn.3079
- Lee, D. A., Yoo, S., Pak, T., Salvatierra, J., Velarde, E., Aja, S., et al. (2014). Dietary and sex-specific factors regulate hypothalamic neurogenesis in young adult mice. *Front. Neurosci.* 8:157. doi: 10.3389/fnins.2014.00157
- Lein, E. S., Hawrylycz, M. J., Ao, N., Ayres, M., Bensinger, A., Bernard, A., et al. (2007). Genome-wide atlas of gene expression in the adult mouse brain. *Nature* 445, 168–176.
- Lustig, M., Erskine, L., Mason, C. A., Grumet, M., and Sakurai, T. (2001). NrCAM expression in the developing mouse nervous system: ventral midline structures, specific fiber tracts, and neuropilar regions. *J. Comp. Neurol.* 434, 13–28. doi: 10.1002/cne.1161
- Maness, P. F., and Schachner, M. (2007). Neural recognition molecules of the immunoglobulin superfamily: signaling transducers of axon guidance and neuronal migration. *Nat. Neurosci.* 10, 19–26. doi: 10.1038/nn1827
- Marthiens, V., Kazanis, I., Moss, L., Long, K., and Ffrench-Constant, C. (2010). Adhesion molecules in the stem cell niche—more than just staying in shape? *J. Cell Sci.* 123, 1613–1622. doi: 10.1242/jcs.054312
- Messina, A., and Giacobini, P. (2013). Semaphorin signaling in the development and function of the gonadotropin hormone-releasing hormone system. *Front. Endocrinol.* 4:133. doi: 10.3389/fendo.2013.00133
- Miranda-Angulo, A. L., Byerly, M. S., Mesa, J., Wang, H., and Blackshaw, S. (2014). Rax regulates hypothalamic tanycyte differentiation and barrier function in mice. *J. Comp. Neurol.* 522, 876–899. doi: 10.1002/cne.23451
- Morante-Redolat, J. M., and Porlan, E. (2019). Neural stem cell regulation by adhesion molecules within the subependymal niche. *Front. Cell Dev. Biol.* 7:102. doi: 10.3389/fcell.2019.00102
- Moy, S. S., Nonneman, R. J., Young, N. B., Demyanenko, G. P., and Maness, P. F. (2009). Impaired sociability and cognitive function in NrCam-null mice. *Behav. Brain Res.* 205, 123–131. doi: 10.1016/j.bbr.2009.06.021
- Müller-Fielitz, H., Stahr, M., Bernau, M., Richter, M., Abele, S., Krajka, V., et al. (2017). Tanycytes control the hormonal output of the hypothalamic-pituitary-thyroid axis. *Nat. Commun.* 8:484. doi: 10.1038/s41467-017-00604-6
- Nishino, J., Yamashita, K., Hashiguchi, H., Fujii, H., Shimazaki, T., and Hamada, H. (2004). Meteorin: a secreted protein that regulates glial cell differentiation and promotes axonal extension. *EMBO J.* 23, 1998–2008. doi: 10.1038/sj.emboj.7600202
- Noctor, S. C., Flint, A. C., Weissman, T. A., Dammerman, R. S., and Kriegstein, A. R. (2001). Neurons derived from radial glial cells establish radial units in neocortex. *Nature* 409, 714–720. doi: 10.1038/35055553
- Ohyama, K., Ellis, P., Kimura, S., and Placzek, M. (2005). Directed differentiation of neural cells to hypothalamic dopaminergic neurons. *Development* 132, 5185–5197. doi: 10.1242/dev.02094
- Park, M. H., Son, D. J., Nam, K. T., Kim, S. Y., Oh, S. Y., Song, M. J., et al. (2016). PRDX6 inhibits neurogenesis of neural precursor cells through downregulation of wdfy1 mediated TLR4 signal. *bioRxiv* [Preprint]. doi: 10.1101/086371
- Parkash, J., Messina, A., Langlet, F., Cimino, I., Loyens, A., Mazur, D., et al. (2015). Semaphorin7A regulates neuroglial plasticity in the adult hypothalamic median eminence. *Nat. Commun.* 6:6385. doi: 10.1038/ncomms7385
- Placzek, M., and Dale, K. (1999). Tissue recombinations in collagen gels. *Methods Mol. Biol.* 97, 293–304. doi: 10.1385/1-59259-270-8:293
- Placzek, M., Fu, T., and Towers, M. (2020). Development of the neuroendocrine hypothalamus. *Masterclass Neuroendocrinol.* 23, 257–291. doi: 10.1007/978-3-030-40002-6_1
- Placzek, M., Jessell, T. M., Dodd, J. (1993). Induction of floor plate differentiation by contact-dependent, homeogenetic signals. *Development* 117, 205–218. doi: 10.1242/dev.117.1.205
- Prevot, V., Dehouck, B., Sharif, A., Ciofi, P., Giacobini, P., and Clasadonte, J. (2018). The versatile tanycyte: a hypothalamic integrator of reproduction and energy metabolism. *Endocr. Rev.* 39, 333–368. doi: 10.1210/er.2017-00235
- Quartier, A., Chatrousse, L., Redin, C., Keime, C., Haumesser, N., Maglott-Roth, A., et al. (2018). Genes and pathways regulated by androgens in human neural cells, potential candidates for the male excess in autism spectrum disorder. *Biol. Psychiatry* 84, 239–252. doi: 10.1016/j.biopsych.2018.01.002
- Robins, S. C., Stewart, I., McNay, D. E., Taylor, V., Giachino, C., Goetz, M., et al. (2013). α -Tanycytes of the adult hypothalamic third ventricle include distinct populations of FGF-responsive neural progenitors. *Nat. Commun.* 4:2049. doi: 10.1038/ncomms3049

- Rodríguez, E., Guerra, M., Peruzzo, B., and Blázquez, J. L. (2019). Tanycytes: a rich morphological history to underpin future molecular and physiological investigations. *J. Neuroendocrinol.* 31:e12690. doi: 10.1111/jne.12690
- Rohrbach, A., Caron, E., Dali, R., Brunner, M., Pasquettaz, R., Kolotuev, I., et al. (2021). Ablation of glucokinase-expressing tanycytes impacts energy balance and increases adiposity in mice. *Mol. Metab.* 53:101311. doi: 10.1016/j.molmet.2021.101311
- Romanov, R. A., Zeisel, A., Bakker, J., Girach, F., Hellysaz, A., Tomer, R., et al. (2017). Molecular interrogation of hypothalamic organization reveals distinct dopamine neuronal subtypes. *Nat. Neurosci.* 20, 176–188. doi: 10.1038/nn.4462
- Sakurai, T. (2012). The role of NrCAM in neural development and disorders—beyond a simple glue in the brain. *Mol. Cell. Neurosci.* 49, 351–363. doi: 10.1016/j.mcn.2011.12.002
- Sakurai, T., Lustig, M., Babiarz, J., Furley, A. J., Tait, S., Brophy, P. J., et al. (2001). Overlapping functions of the cell adhesion molecules Nr-CAM and L1 in cerebellar granule cell development. *J. Cell Biol.* 154, 1259–1273. doi: 10.1083/jcb.200104122
- Sakurai, T., Ramoz, N., Reichert, J. G., Corwin, T. E., Kryzak, L., Smith, C. J., et al. (2006). Association analysis of the NrCAM gene in autism and in subsets of families with severe obsessive-compulsive or self-stimulatory behaviors. *Psychiatr. Genet.* 16, 251–257. doi: 10.1097/01.ypg.0000242196.81891.c9
- Salvatierra, J., Lee, D. A., Zibetti, C., Duran-Moreno, M., Yoo, S., Newman, E. A., et al. (2014). The LIM homeodomain factor Lhx2 is required for hypothalamic tanycyte specification and differentiation. *J. Neurosci.* 34, 16809–16820. doi: 10.1523/JNEUROSCI.1711-14.2014
- Samms, R. J., Lewis, J. E., Lory, A., Fowler, M. J., Cooper, S., Warner, A., et al. (2015). Antibody-mediated inhibition of the FGFR1c isoform induces a catabolic lean state in siberian hamsters. *Curr. Biol.* 25, 2997–3003. doi: 10.1016/j.cub.2015.10.010
- Shimogori, T., Lee, D. A., Miranda-Angulo, A., Yang, Y., Wang, H., Jiang, L., et al. (2010). A genomic atlas of mouse hypothalamic development. *Nat. Neurosci.* 13, 767–775. doi: 10.1038/nn.2545
- Sild, M., and Ruthazer, E. S. (2011). Radial glia: progenitor, pathway, and partner. *Neuroscientist* 17, 288–302. doi: 10.1177/1073858410385870
- Silva-Vargas, V., Crouch, E. E., and Doetsch, F. (2013). Adult neural stem cells and their niche: a dynamic duo during homeostasis, regeneration, and aging. *Curr. Opin. Neurobiol.* 23, 935–942. doi: 10.1016/j.conb.2013.09.004
- Tamamaki, N., Nakamura, K., Okamoto, K., and Kaneko, T. (2001). Radial glia is a progenitor of neocortical neurons in the developing cerebral cortex. *Neurosci. Res.* 41, 51–60. doi: 10.1016/s0168-0102(01)00259-0
- Xenaki, D., Martin, I. B., Yoshida, L., Ohyama, K., Gennarini, G., Grumet, M., et al. (2011). F3/contactin and TAG1 play antagonistic roles in the regulation of sonic hedgehog-induced cerebellar granule neuron progenitor proliferation. *Development* 138, 519–529. doi: 10.1242/dev.051912
- Yoo, S., and Blackshaw, S. (2018). Regulation and function of neurogenesis in the adult mammalian hypothalamus. *Prog. Neurobiol.* 170, 53–66. doi: 10.1016/j.pneurobio.2018.04.001
- Yoo, S., Cha, D., Kim, S., Jiang, L., Cooke, P., Adebisin, M., et al. (2020). Tanycyte ablation in the arcuate nucleus and median eminence increases obesity susceptibility by increasing body fat content in male mice. *Glia* 68, 1987–2000. doi: 10.1002/glia.23817
- Yoo, S., Kim, J., Lyu, P., Hoang, T. V., Ma, A., Trinh, V., et al. (2021). Control of neurogenic competence in mammalian hypothalamic tanycytes. *Sci. Adv.* 7:eabg3777. doi: 10.1126/sciadv.abg3777
- Zonta, B., Desmazieres, A., Rinaldi, A., Tait, S., Sherman, D. L., Nolan, M. F., et al. (2011). A critical role for Neurofascin in regulating action potential initiation through maintenance of the axon initial segment. *Neuron* 69, 945–956. doi: 10.1016/j.neuron.2011.02.021

Conflict of Interest: The authors declare that the research was conducted in the absence of any commercial or financial relationships that could be construed as a potential conflict of interest.

Publisher's Note: All claims expressed in this article are solely those of the authors and do not necessarily represent those of their affiliated organizations, or those of the publisher, the editors and the reviewers. Any product that may be evaluated in this article, or claim that may be made by its manufacturer, is not guaranteed or endorsed by the publisher.

Copyright © 2022 Moore, Chinnaiya, Kim, Brown, Stewart, Robins, Dowsett, Muir, Travaglio, Lewis, Ebling, Blackshaw, Furley and Placzek. This is an open-access article distributed under the terms of the Creative Commons Attribution License (CC BY). The use, distribution or reproduction in other forums is permitted, provided the original author(s) and the copyright owner(s) are credited and that the original publication in this journal is cited, in accordance with accepted academic practice. No use, distribution or reproduction is permitted which does not comply with these terms.